JOURNAL OF GEOPHYSICAL RESEARCH, VOL. 105, NO. C3, PAGES 6591–6610, MARCH 15, 2000

A model of sediment resuspension and transport dynamics in southern Lake Michigan

Jing Lou and David J. Schwab
NOAA Great Lakes Environmental Research Laboratory, Ann Arbor, Michigan

Dmitry Beletsky[1]
Department of Naval Architecture and Marine Engineering, University of Michigan, Ann Arbor

Nathan Hawley
NOAA Great Lakes Environmental Research Laboratory, Ann Arbor, Michigan

Abstract. A quasi-three-dimensional suspended sediment transport model was developed and generalized to include combined wave-current effects to study bottom sediment resuspension and transport in southern Lake Michigan. The results from a three-dimensional circulation model and a wind wave model were used as input to the sediment transport model. Two effects of nonlinear wave-current interactions were considered in the sediment transport model: the changes in turbulence intensity due to waves and the enhancement of induced bottom shear stresses. Empirical formulations of sediment entrainment and resuspension processes were established and parameterized by laboratory data and field studies in the lake. In this preliminary application of the model to Lake Michigan, only a single grain size is used to characterize the sedimentary material, and the bottom of the lake is treated as an unlimited sediment source. The model results were compared with measured suspended sediment concentrations at two stations and several municipal water intake turbidity measurements in southern Lake Michigan during November–December 1994. The model was able to reproduce the general patterns of high-turbidity events in the lake. A model simulation for the entire 1994–1995 two-year period gave a reasonable description of sediment erosion/deposition in the lake, and the modeled settling mass fluxes were consistent with sediment trap data. The mechanisms of sediment resuspension and transport in southern Lake Michigan are discussed. To improve the model, sediment classifications, spatial bottom sediment distribution, sediment source function, and tributary sediment discharge should be considered.

1. Introduction

The presence of contaminated sediments in Lake Michigan poses a serious environmental problem with long-term consequences to the population and economy of nearby states. For many constituents in the Great Lakes, sediment resuspension results in much greater fluxes than from external inputs [*Eadie et al*., 1984; *Eadie and Robbins*, 1987; *Robbins and Eadie*, 1991; *Brooks and Edgington*, 1994]. Therefore fragile ecosystems may be threatened by the redistribution of sediments and the associated transport of contaminants. In the past few years, satellite images illustrated an annually occurring major sediment resuspension event in Lake Michigan in late winter and early spring: a sediment plume ~10 km wide extending over 200 km along the southern shore of the lake [*Eadie et al*., 1996]. Despite the significant scale of that event, the dominant mechanisms for sediment resuspension and transport in the lake are not well known, and there is still a lack of fundamental knowledge in this field.

The sediment distribution in Lake Michigan is markedly nonhomogeneous. Silt and sand cover most of the lake bottom. Generally, the coarse sand is found along the shoreline, and more fine-grained sediment is located offshore. Sand and muddy sand cover the southwestern corner of the southern basin [*Colman and Foster*, 1994], an area corresponding to the water depth <30 m (Figure 1). In southern Lake Michigan, fine sediments are mainly located in the eastern part at water depths >30 m.

Recently, there has been a growing interest in sediment resuspension problems in the Great Lakes. *Lesht and Hawley* [1987], *Hawley and Lesht* [1995], *Hawley and Lee* [1999], and *Lee and Hawley* [1998] used instrumented tripods to make continuous observations of current, temperature, and turbidity in southern Lake Michigan. It was shown that during the stratified period the water turbidity is lower, though high levels of sediment concentration may sometimes occur due to episodic mixing during upwellings. In the unstratified period the lake is well mixed, and higher turbidities were observed due to winter storms.

Long-term sediment flux trap studies in Lake Michigan were made by *Eadie et al*. [1984, 1994] and *Robbins and Eadie* [1991]. The seasonal changes in mass flux and the resuspension rates

[1]Also at Cooperative Institute for Limnology and Ecosystem Research, NOAA Great Lakes Environmental Research Laboratory and University of Michigan, Ann Arbor.

Copyright 2000 by the American Geophysical Union.

Paper number 1999JC900325.
0148-0227/00/1999JC900325$09.00

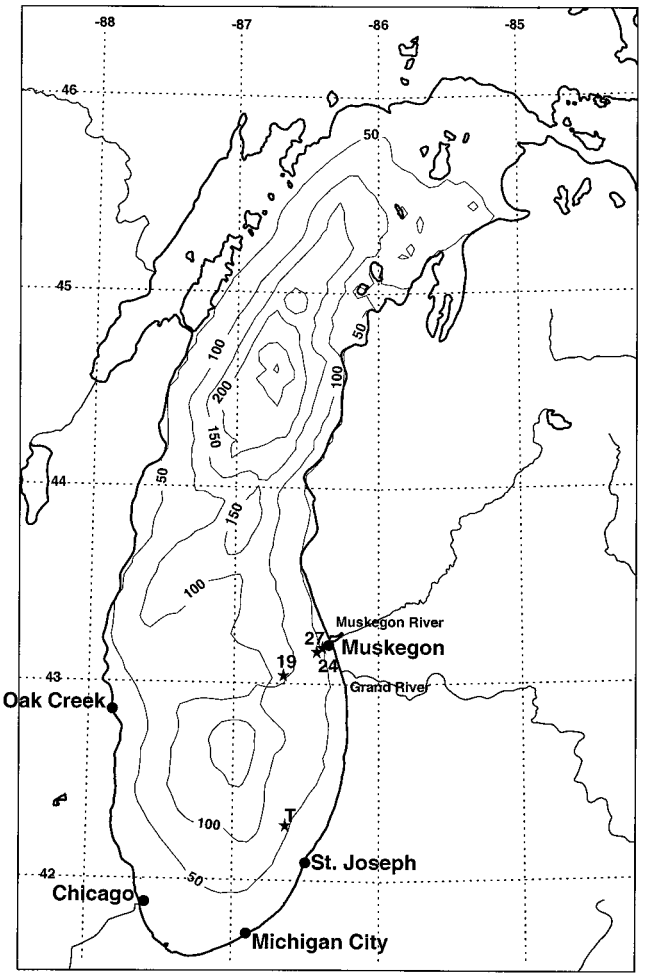

Figure 1. Tripod locations (19, 24, 27), sediment trap mooring (T), and water intake locations in Lake Michigan. Depth contours are in meters.

of phosphorus, PCBs, and organic carbon from sediment traps were estimated. Erosion properties of Lake Michigan sediments were measured by the Sedflume, a water flume designed for measuring erosion rate under different shear stresses [*Taylor et al*., 1996].

To study the effects of sediment transport in the Great Lakes, it is necessary to understand and predict the sediment concentration and fate of these sediments using numerical models. A two-dimensional sediment transport model was applied to Green Bay, the Lower Fox River [*Ziegler and Lick*, 1986, 1988; *Gailani et al*., 1991], Lake Erie [*Lick et al*., 1994], and the Pawtuxet River, Rhode Island [*Ziegler and Nisbet*, 1994], to study sediment entrainment and resuspension properties. In that model, sediment mixtures were divided into three different classes: noncohesive coarse particles; very fine-grained particles with zero settling speed; and cohesive fine-grained sediment particles. The sediment compaction effect was also incorporated. The model realistically simulated fine-grained sediment resuspension, deposition, and transport in shallow waters during storms. *Lee et al*. [1994] used a similar model to study deposition and erosion in Sandusky Bay, Ohio. However, such depth-integrated models neglect the important three-dimensional transport mechanisms in sediment resuspension processes. Considering the complications of three-dimensional models, a quasi-three-dimensional (3-D) model can be a more efficient tool for sediment resuspension and transport modeling.

In this paper, sediment resuspension, deposition, and transport in southern Lake Michigan (where a well-defined data record is available) were examined with a quasi-3-D numerical sediment transport model. Circulation model and wind wave model results were used as hydrodynamic input. The parameters and empirical relations needed in the model were calibrated by field measurements and laboratory data. The model application to southern Lake Michigan is illustrated by comparing suspended sediment concentration results with in situ measurements and water intake turbidity data, vertical mass fluxes measured by sediment traps, satellite sediment plume imagery, and erosion-deposition distributions. The main mechanisms of sediment resuspension and transport in southern Lake Michigan are discussed.

The outline of this paper is as follows: the sediment transport model is described in section 2, Lake Michigan hydrodynamics are briefly described in section 3, numerical simulations of sediment resuspension events in November–December 1994 are presented in section 4, the 1994–1995 two-year model simulations are included in section 5, a summary is given in section 6, and the model equations are given in the appendix.

2. Suspended Sediment Transport Model

A quasi-3-D suspended sediment transport model based on the convection-diffusion equation has been developed. It is based on the work of *Galappatti and Vreugdenhil* [1985], who introduced an asymptotic solution to a two-dimensional vertical model for uniform flow. In the present model this approach was developed into more complicated flow fields and generalized to combined wave-current interactions. A similar model was used to describe the coarse suspended sediment transport in Cleveland Bay, Australia, under tidal and wave conditions [*Lou and Ridd*, 1997], as well as fine sediment resuspension processes in the Oder Estuary, a nearly enclosed bay in northern Germany [*Lou et al*., 1999].

The wave effect is taken into account by assuming an analogy of the mixing profile on a wave-averaged and turbulence-averaged scale [*Van Rijn*, 1985]. The enhanced bottom shear stresses are calculated by a nonlinear wave-current bottom boundary layer model [*Lou and Ridd*, 1996]. For cases where the suspended load is the main mode of sediment transport an asymptotic solution of the convection-diffusion equation is used. The vertical concentration structure has been shown to depend only on the vertical velocity profile and the mixing coefficient and can be calculated in advance. The three-dimensional concentration is represented in terms of depth-averaged concentration and its horizontal derivatives. As a result, the three-dimensional sediment transport problem is reduced to a quasi-3-D model: a two-dimensional depth-averaged sediment transport model with the associated vertical concentration profiles being solved in advance.

The suspended particles are assumed to be so small that their motions relative to the ambient fluid fall into the Stokes range. The velocities of sediment particles are set equal to the flow velocities (u, v) in the (x, y) directions, except in the vertical direction z, where sediment settling velocity w_s should be taken into account. The basic equation describing mass

conservation of suspended sediment in a turbulent flow can be expressed as

$$\frac{\partial c}{\partial t} + u\frac{\partial c}{\partial x} + v\frac{\partial c}{\partial y} + (w - w_s)\frac{\partial c}{\partial z} = \frac{\partial}{\partial x}\left(\varepsilon_x \frac{\partial c}{\partial x}\right) + \frac{\partial}{\partial y}\left(\varepsilon_y \frac{\partial c}{\partial y}\right) + \frac{\partial}{\partial z}\left(\varepsilon_z \frac{\partial c}{\partial z}\right), \quad (1)$$

where ε_x, ε_y, ε_z are sediment particle diffusion coefficients in x, y, z directions for the combined motion of waves and currents, and $c(x, y, z, t)$ is the suspended sediment concentration.

It is assumed that in the equilibrium condition the concentration distribution is determined mainly by the balance between diffusion and particle settling. This equilibrium concentration represents the zeroth-order approximation to the concentration field. Under this assumption and further simplifications, an asymptotic solution of (1) has been derived. The details of the model equations are given in the appendix.

The model solves the 3-D convection-diffusion concentration equation with almost the same efficiency as that of 2-D horizontal models. It has been shown that higher-order solutions decrease rapidly compared to the first-order approximation [*Lou*, 1995]. The deviation between the first-order estimation and the exact solution depends mainly on the ratio of $w_s/\varepsilon_{\max}$ (where $\varepsilon_{\max}$ is the maximum value of the vertical diffusion coefficient), and this deviation increases as $w_s/\varepsilon_{\max}$ increases. More discussions on the validity conditions of the asymptotic solution are given by *Wang and Ribberink* [1986] and *Lou* [1995]. To reduce numerical dispersion, the second-order upwind difference scheme was applied to the horizontal advection terms. A hybrid multistage Crank-Nicolson and alternating direction implicit (ADI) solution scheme was developed to calculate the sediment concentration results. In the model application to Lake Michigan a uniform 5 km horizontal grid mesh, 20 vertical layers, and a staggered C-grid arrangement were employed for the sediment transport model. The same grid is used for the circulation and wind wave model. More details of the numerical scheme have been given by *Lou* [1995]. In addition to the generalized flow regime the nonlinear wave-current interactions have also been considered. The wave-current interaction has two significant effects on sediment transport: (1) changes in eddy viscosity, which represent changes in turbulence intensity, and (2) enhancement in bottom shear stresses. These are discussed in sections 2.1–2.3.

2.1. Vertical Diffusion Under Wave-Current Interaction

In many practical applications the horizontal diffusion effects are small when compared with the vertical diffusion. In this study a constant horizontal diffusion coefficient has been assumed. Only the vertical diffusion coefficient for sediment particles is calculated. The sediment particle diffusion is different from fluid diffusion due to different effective particle mixing lengths, the diffusion rate, and the damping effect. However, for most practical situations where suspended sediment transport is the main mode of motion ($w_s/u_* \ll 1$, where u_* is the bed shear velocity) and sediment concentration is relatively low, the sediment mixing coefficient can be estimated by the fluid diffusion.

The following three-layer wave diffusion coefficient was proposed by *Van Rijn* [1986], based on wave-induced sediment concentration distribution data [*Bosman*, 1982]:

$$\varepsilon_w = \begin{cases} \varepsilon_{w,\text{bed}} = 6.5 \times 10^{-4}\alpha_b \delta D_*^2 u_{\text{orb}} & z \le \delta \\ \varepsilon_{w,\max} = 3.5 \times 10^{-2}\alpha_b \dfrac{hH_s}{T} & z \ge 0.5h \\ \varepsilon_{w,\text{bed}} + (\varepsilon_{w,\max} - \varepsilon_{w,\text{bed}})\dfrac{z - \delta}{0.5h - \delta} & \delta < z < 0.5h, \end{cases} \quad (2)$$

in which ε_w is the wave-induced diffusion coefficient, $\varepsilon_{w,\text{bed}}$ is the wave-induced diffusion coefficient within the wave bottom boundary layer, $\varepsilon_{w,\max}$ is the maximum wave-induced diffusion coefficient, which applies to the upper half of the water column, δ is the thickness of the near bed mixing layer (or wave bottom boundary layer thickness), h is the water depth, H_s is the significant wave height, T is the wave period, u_{orb} is the near bottom orbital velocity, α_b is the wave breaking coefficient, and D_* is a dimensionless particle size parameter, which is related to the median sediment particle size D_{50} as

$$D_* = D_{50}\left(\frac{(s-1)g}{\nu^2}\right)^{1/3}, \quad (3)$$

where $s = \rho_s/\rho$ is the specific density, ρ_s is the sediment density, ρ is the water density, and ν is the kinematic viscosity.

The square of the sediment mixing coefficient due to the combination of waves and currents is assumed to be given by the sum of the squares of the current-related and wave-related values [*Van Rijn*, 1989; *Rakha et al*., 1997]:

$$\varepsilon_z^2 = \varepsilon_c^2 + \varepsilon_w^2. \quad (4)$$

The current-related diffusion coefficient ε_c is calculated numerically from a 3-D circulation model using a turbulence closure scheme. The approach used in (4) corresponds to the summation of kinetic energy of both wave and current motions as $\varepsilon \sim lE^{1/2}$, in which E is the kinetic energy and l is the mixing length scale.

2.2. Wave-Current Bottom Shear Stresses

The bottom shear stress required in the sediment transport study is calculated by a bottom boundary layer model. The resulting stress is then used in the bottom boundary condition for the sediment transport model. The effect of wave-current interaction on the bottom shear stress is calculated based on the concept of *Grant and Madsen* [1979] in an iterative form. A similar method was used by *Signell et al*. [1990], but with a different definition of wave friction.

The maximum bottom stress $\tau_{b,\max}$ for wave-current combination is defined as

$$\tau_{b,\max} = \tfrac{1}{2} f_{cw}\rho(U_\delta^2 + u_c^2 + 2U_\delta u_c \cos\phi_c), \quad (5)$$

in which ρ is the water density, f_{cw} is an effective friction factor, U_δ is the maximum near bottom wave orbital velocity determined from linear wave theory, u_c is the mean bottom current, and ϕ_c is the angle between wave propagation and current direction.

The calculation of the effective friction coefficient f_{cw} begins by determining the oscillatory component of the stress τ_w, which can be determined from

$$\tau_w = \rho u_{*w}^2 = \tfrac{1}{2}\rho f_w U_\delta^2, \quad (6)$$

where f_w is the wave friction factor. Its value can be obtained by using *Jonsson*'s [1966] relation

$$f_w = \exp\,[-6 + 5.2(A_\delta/k_s)^{-0.19}]$$
$$f_{w,\max} = 0.3 \qquad A_\delta/k_s \le 1.57, \tag{7}$$

where k_s is the physical bottom roughness and A_δ is the near-bottom excursion amplitude.

With u_{*w} determined, an iterative procedure is used to calculate f_{cw} at the upper edge of the wave-current boundary layer as follows:

1. Starting with an initial guess of f_{cw}, the steady shear velocity component u_{*c} is obtained by

$$u_{*c} = \sqrt{f_{cw}}u_c. \tag{8}$$

2. The combined wave-current friction velocity u_{*cw} is defined as

$$u_{*cw} = \sqrt{\tau_{b,\max}/\rho} \tag{9}$$

and can be obtained by the wave-related and current-related friction velocities:

$$u_{*cw} = (u_{*c}^2 + u_{*w}^2 + 2u_{*c}u_{*w}\cos\,\phi_c)^{1/2}. \tag{10}$$

3. To determine the effective bottom roughness k_b,

$$k_b = k_s\left[24\,\frac{u_{*cw}}{U_\delta}\frac{A_\delta}{k_s}\right]^{[1-(u_{*c}/u_{*cw})]}. \tag{11}$$

4. The effective roughness is then used to calculate the velocity profile in the boundary layer:

$$u = \frac{u_{*c}}{\kappa}\ln\left(\frac{z}{k_b/30}\right). \tag{12}$$

5. Solving for the velocity at a reference level, a new estimate of the friction coefficient is obtained:

$$f_{cw} = \left[\frac{\kappa}{\ln\,(30\delta_{cw}/k_b)}\right]^2. \tag{13}$$

The above procedure (1)–(5) is repeated until the successive estimates of f_{cw} differ by less than a preset error value (10^{-6} in this work).

2.3. Bottom Boundary Conditions for Sediment Transport

The location of the fluid-sediment interface has been averaged over the wavelength of bedforms such as ripples or dunes. If the reference location $z = a$ is chosen sufficiently close to the boundary, the vertical fluid velocity w can be neglected. As a result, the upward flux of suspended sediment, evaluated at a reference distance $z = a$ above the bed, can be given by

$$F_a = w_s(E_s - c_a\cos\,\theta), \tag{14}$$

where c_a is the near-bed suspended sediment concentration, $w_s c_a \cos\,\theta$ is the deposition rate per unit bed area due to the settling velocity w_s, θ is the bottom slope, and E_s is a dimensionless coefficient describing the entrainment of bottom sediment into suspension due to turbulence. If the bed slope is small, the net upward flux at the bed can be approximated by

$$F_a = w_s(E_s - c_a). \tag{15}$$

To solve for the mass flux of suspended sediment at the bottom, it is necessary to specify the values of E_s and c_a at the reference bottom boundary.

2.3.1. Bottom concentration. A formula for noncohesive suspended sediment concentration c_a at reference level $z = a$ above the bed is given by *Van Rijn* [1989]:

$$c_a = 0.015\,\frac{D_{50}}{a}\frac{T^n}{D_*^{0.3}}, \tag{16}$$

in which T is the bed shear stress parameter, $T = (\tau_b - \bar{\tau}_{b,cr})/\bar{\tau}_{b,cr}$, τ_b is the effective bed shear stress under combined waves and current, which can be calculated by the approach given in the previous section, and $\bar{\tau}_{b,cr}$ is the Shields critical bed shear stress for sediment suspension, a value which should be obtained by field data or laboratory measurement. The exponent n was set to 1.5 for noncohesive coarse sediment in previous applications. We found that when using this value, the model will overestimate the sediment concentration in southern Lake Michigan because of the cohesion and compaction properties of the sediment there. In southern Lake Michigan the erosion rate for surficial sediment is found to change in an approximately linear relationship with shear stress in laboratory experiments [*Taylor et al.*, 1996]. So an exponent value of $n = 1.0$ is used in the above equation for Lake Michigan. A specified value of bottom concentration (equation (16)) was used as the bottom boundary condition, while the flux relation (equation (15)) is used to estimate instantaneous values of erosion or deposition at the lake bottom. This is the bottom boundary condition for an unlimited bed sediment source. If the sediment erosion on the bed is limited, a probability function representing the sediment suspension rate should be included in (16).

2.3.2. Entrainment coefficient. *Garcia and Parker* [1991] developed an empirical relation for the entrainment coefficient, and this new relation has been generalized to sediment mixtures with the aid of field data. This empirical fit can provide reasonable estimates of the entrainment coefficient. As a result, a similar relation for uniform grain size is adopted in our study as follows:

$$E_s = \frac{AZ^5}{1 + \dfrac{A}{0.3}Z^5}, \tag{17}$$

where

$$Z = \frac{u_*}{w_s}R^{0.6} \tag{18}$$

$$R = \frac{\sqrt{(s-1)gD}}{\nu}D, \tag{19}$$

where A is an empirical parameter of 1.3×10^{-7}, D is the size of bottom sediment, u_* is the bottom shear velocity, E_s is the sediment entrainment coefficient, and w_s is the settling velocity of sediment.

3. Hydrodynamics of Lake Michigan

3.1. Circulation

Circulation in Lake Michigan (and the other Great Lakes) is highly episodic since it is primarily wind-driven. The most energetic currents and waves occur during winter and spring storms, when temperature gradients in the lake are lowest and winds are strongest. The characteristic wind-driven circulation pattern in a lake consists of two counter-rotating gyres, a coun-

terclockwise-rotating (cyclonic) gyre to the right of the wind and a clockwise-rotating (anticyclonic) gyre to the left [*Bennett*, 1974]. This simple two-gyre circulation pattern can be modified by asymmetry in the lake's bathymetry, stratification, or vorticity in the wind field. In the southern basin of Lake Michigan, alongshore currents are initially driven by pulses of wind but can subsequently reverse direction as the characteristic two-gyre wind-driven circulation pattern rotates cyclonically around the basin as a vorticity wave [*Saylor et al*., 1980; *Schwab*, 1983]. The relaxation time of this response is determined by the lowest mode topographic wave period of the basin [*Saylor et al*., 1980], which is typically of the order of several days. Because the predominant winds are from the west, wind-driven circulation in the southern basin is more frequently cyclonic than anticyclonic.

A Great Lakes version of the three-dimensional Princeton ocean model (POM) [*Blumberg and Mellor*, 1987] was applied to Lake Michigan for the 2-year period 1994–1995. The model is hydrostatic and Boussinesq. It uses wind stress and heat flux forcing at the surface, free-slip lateral boundary conditions, and quadratic bottom friction. When applied to the Great Lakes, the salinity is set to a constant low value of 0.2 ppt. The model includes the *Mellor and Yamada* [1982] level 2.5 turbulence closure parameterization. The model with its Mellor-Yamada turbulence scheme has been successfully tested in numerous circulation applications including the Hudson-Raritan Estuary [*Oey et al*., 1985], Delaware Bay [*Galperin and Mellor*, 1990], and also in bottom boundary layer modeling by *Weatherly and Martin* [1978] and *Mellor* [1986]. The hydrodynamic model of Lake Michigan uses 20 vertical levels and a uniform horizontal grid size of 5 km. The temperature field was initialized on April 1, 1994, with uniform temperature of 2°C. This is typical for the Great Lakes in early spring when the lakes are well mixed due to fall and winter convection. The model was driven by surface heat fluxes and the wind field interpolated from observation data over the lake using the techniques described by *Schwab and Morton* [1984] and *Schwab and Bedford* [1994]. The model was extensively calibrated with various field data (temperature, water level, current velocity) and was able to realistically reproduce the main features of seasonal thermal structure and circulation in Lake Michigan [*Beletsky and Schwab*, 1998; *Schwab and Beletsky*, 1998]. In the present study the output (3-D current field, eddy viscosity, and current-induced bottom stresses) from this model, together with the wind wave model output (described below), is used to provide the forcing input for the sediment transport model.

Unlike highly episodic wind-driven circulation, seasonal circulation in Lake Michigan appears to be more stable. To illustrate seasonal circulation patterns, two 6-month averaged normalized stream functions are shown in Figure 2. The first period (summer) is from May to October 1994, and the second period (winter) is from November 1994 to April 1995, which approximately represent the stratified and unstratified periods in Lake Michigan. Stream function values are normalized by the maximum absolute value which was 55,640 m^3/s for the May to October period and 131,606 m^3/s for the November to April period. Modeled mean circulation was cyclonic in both summer and winter, with cyclonic circulation in subbasins and anticyclonic circulation in shallow southern and northern coastal areas and in midlake ridge areas. In general, modeled winter circulation is stronger and more cyclonic than summer circulation, which is in agreement with observations [*Saylor et al*., 1980; *Gottlieb et al*., 1989]. There are several known mechanisms in the Great Lakes that contribute to resulting cyclonic circulation patterns on seasonal timescales. In summer, cyclonic circulation is supported by onshore-offshore density gradients [*Ayers*, 1956; *Schwab et al*., 1995], stronger downwelling currents than upwelling currents [*Bennett*, 1975], lateral momentum flux in coastal boundary currents [*Csanady*, 1975], and Lagrangian drift associated with internal Kelvin waves [*Wunsh*, 1973]. In winter, quite a different set of factors has been suggested to be responsible for cyclonic circulation in the Great Lakes in the absence of stratification, including nonlinear interaction of topographic waves [*Simons*, 1986] and cyclonic vorticity in the atmosphere [*Rao and Murty*, 1970].

3.2. Waves

Because of strong winds and frequent storms, large wind waves occur more often in the spring and in the ice-free winter than in the summer. With Lake Michigan's orientation, northerly winds generate the largest waves in southern Lake Michigan and therefore the largest energy available for resuspension of nearshore sediment. Northerly winds also contribute to southward transport very near the shore in the southern part of the lake. During the storm of February 1987, wave heights over 5 m were observed at Burns Harbor, Indiana [*Hubertz et al*., 1991].

In this study, a parametric 2-D surface wind wave model for the Great Lakes developed by *Schwab et al*. [1984] was used to provide wave characteristics for use in the sediment transport model. This wind wave model was shown to provide excellent estimates of significant wave height and wave direction for fetch-limited waves [*Liu et al*., 1984; *Schwab and Beletsky*, 1998], though it has a tendency to underestimate wave periods.

3.3. Bottom Shear Stress Distribution

Grant and Madson [1979] showed that in a region where both waves and currents are important, the shear stresses are altered because the turbulence generated by wave-current interaction is different from that expected in the case of pure waves or currents. Currents not capable of transporting sediment on their own may move a considerable amount of sediment if waves are present [*Thorn and Parsons*, 1980]. The bottom shear stress provides an important link between hydrodynamics and sediment transport processes. Figures 3 and 4 give the bottom stress probability distribution for currents only and for the combined effect of waves and currents during 1994–1995. The current and wave data are obtained from the circulation and wind wave models. The threshold shear is taken as 0.1 N/m^2. The bottom shear stress due to nonlinear interaction between waves and current is calculated by the method given in section 2.2. Figures 3 and 4 show the effect of wave-current interaction on the bottom shear stress and the high bottom shear distribution in the lake. The effect of waves occurs mainly in shallow waters in Green Bay and the southern part of the lake. In southern Lake Michigan the wave-current interaction area corresponds to the recurrent sediment plume region [*Eadie et al*., 1996] where bottom shear stress greater than 0.1 N/m^2 occurred over 10% of the time, mainly in winter and spring. It is obvious that both waves and currents play an important role in episodic sediment plume development and transport.

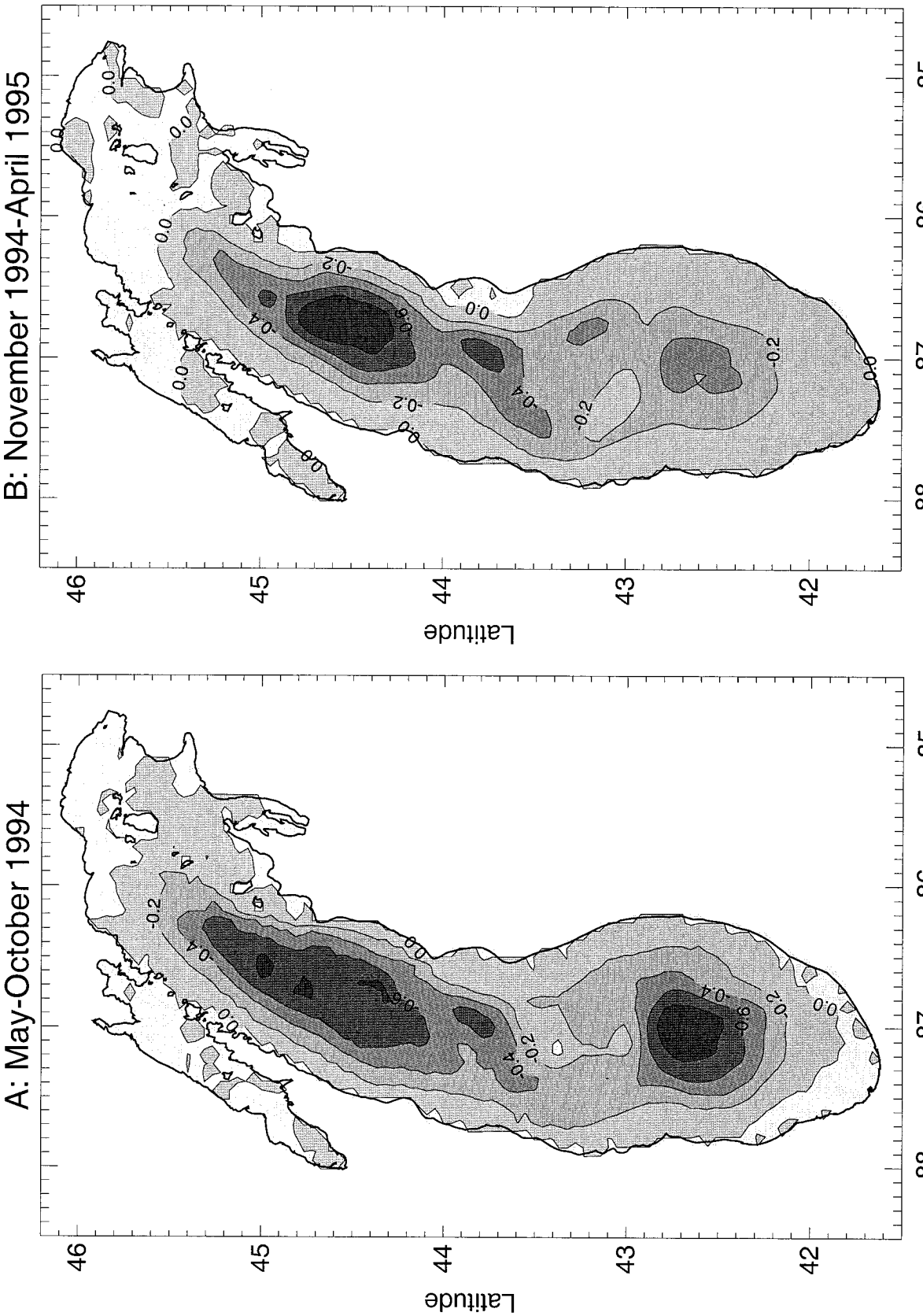

Figure 2. Normalized stream functions for summer and winter circulation in Lake Michigan for (a) May–October 1994 and (b) November 1994 to April 1995 (positive values, clockwise circulation; negative values, counterclockwise circulation).

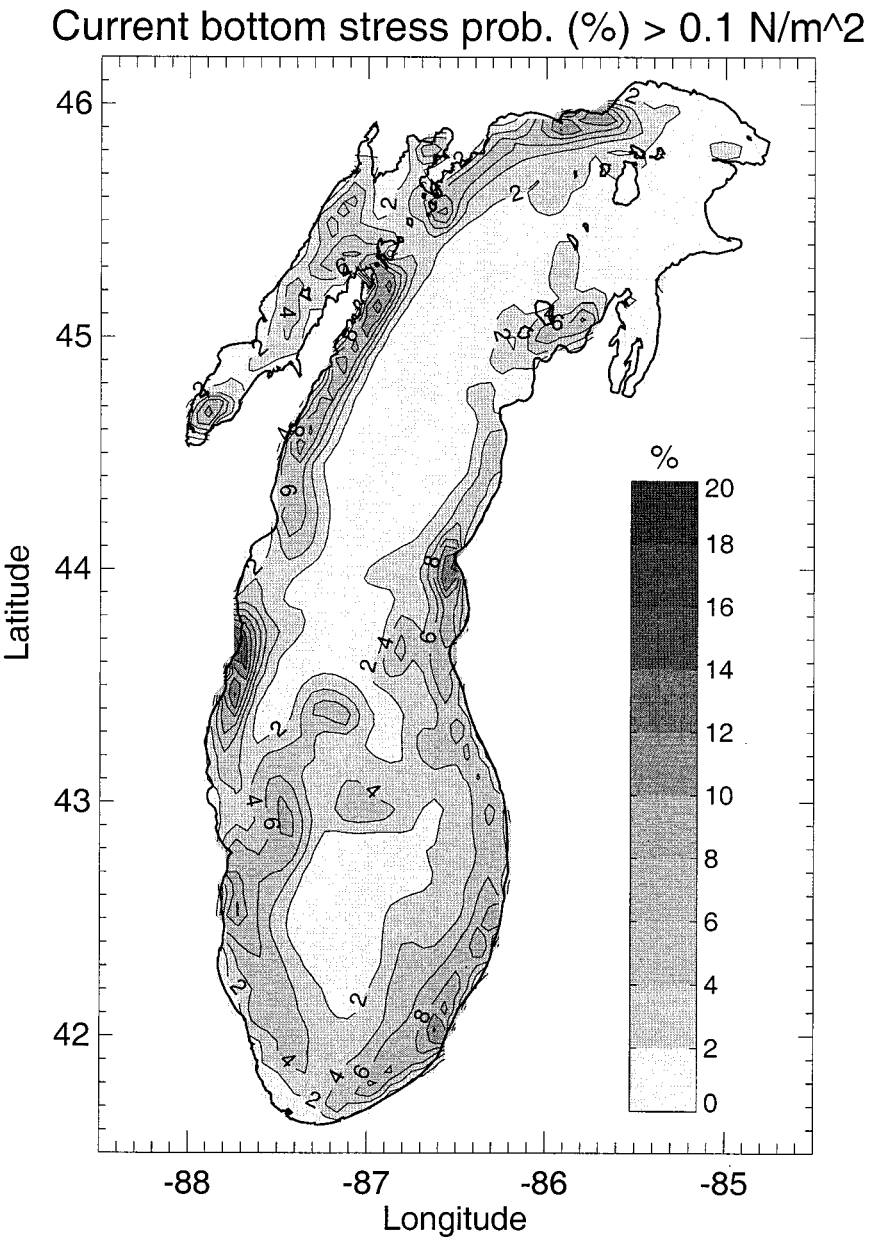

Figure 3. Percentage of time that current-induced bottom stresses exceed 0.1 N/m^2 in Lake Michigan, based on 1994–1995 model results.

4. Numerical Simulation of High-Turbidity Events in November–December 1994

4.1. Field Data

Instrumented moorings were deployed during the winter of 1994–1995 at three stations, 19, 27, and 24 (Figure 1), in southern Lake Michigan to determine the physical processes responsible for sediment resuspension and transport [*Lee and Hawley*, 1998; *Hawley and Lee*, 1999]. The sites were located in water depths of 101, 58, and 28 m, respectively, on a transect running southwest from Muskegon, Michigan. Water depth along the transect increases slowly to 30 m, then more rapidly to ~80 m, after which it increases more gradually. Time series measurements of temperature, current velocity, and water transparency were made at different depths at each station. The transparency readings are reported as beam attenuation coefficient (BAC) from 25-cm path length transmissometers, which generally has a linear relationship with the suspended material concentration in the lake [*Hawley and Zyren*, 1990]. During the above measurements, no resuspension was detected at deep water station 19. So our comparisons with model results are focused on stations 24 and 27. In addition to the sediment concentration measurements at moorings, measurements of water turbidity at five municipal water intakes along southern Lake Michigan were also obtained from water intake plant records. The water intake locations are also shown in Figure 1.

Wind forcing for the hydrodynamic circulation model and the wave model is based on hourly observations from a network of more than 20 meteorological stations around the lake [*Schwab and Beletsky*, 1998]. The winds are adjusted for overwater conditions and interpolated to the 5-km computational grid using a nearest-neighbor technique. The nearest-neighbor

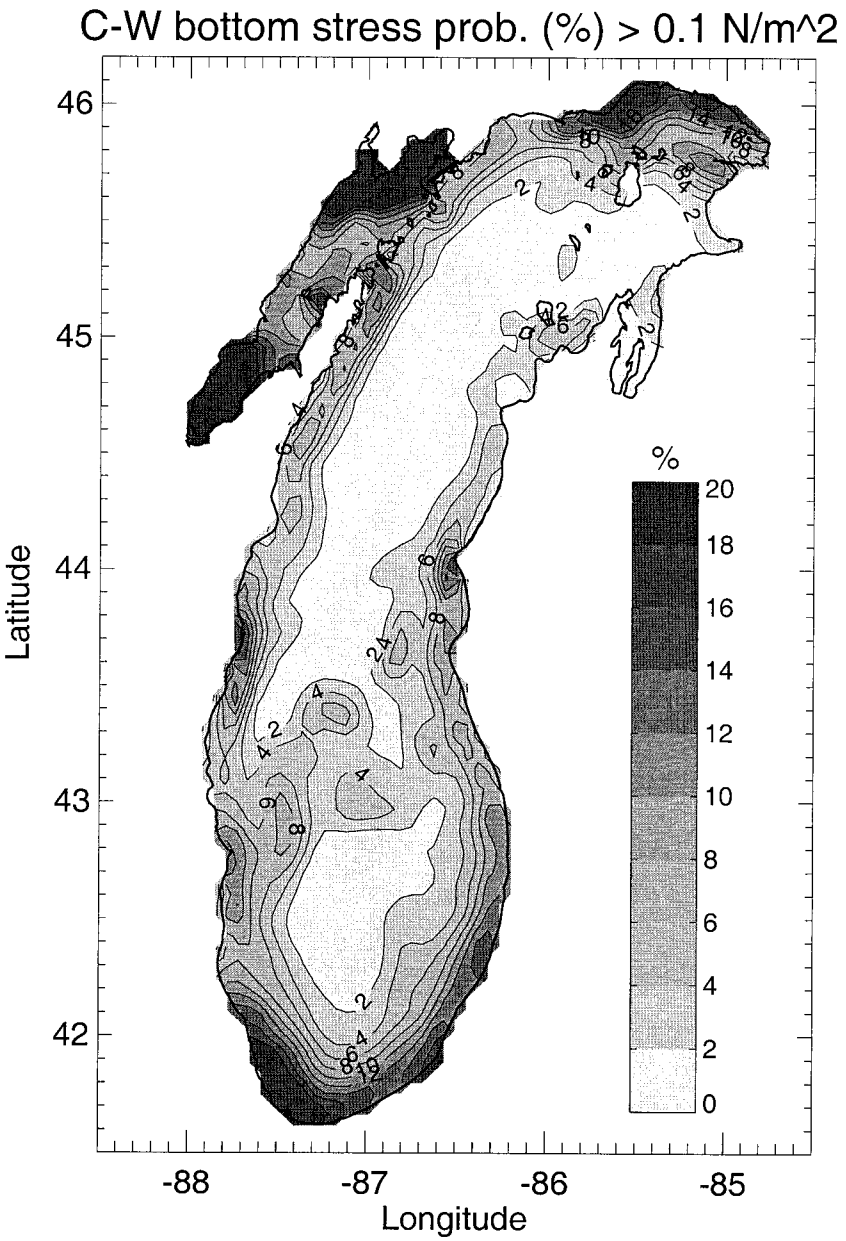

Figure 4. Percentage of time that current-wave induced bottom stresses exceed 0.1 N/m^2 in Lake Michigan, based on 1994–1995 model results.

technique was found to provide similar results to conventional distance-weighted techniques but is computationally more efficient. A time series of the hourly winds at the grid cell nearest to station 24 is shown in Figure 5. There are several occasions when winds exceed 10 m/s, including days 322, 326, and 332. The output from the wave model for this period is shown in Figure 6 in terms of calculated wave height, period, and direction (meteorological convention). Calculated wave heights exceed 3 m, and peak periods are 8–9 s on days 322, 326, and 332. Wave direction generally tends to follow the wind direction. Unfortunately, direct measurements of wave conditions are not available for this time period.

Currents measured 0.5 m above the bottom at station 24 are compared to near-bottom currents calculated by the hydrodynamic model in Figure 7. The measured currents are indicated by the thick line for current components and speed and by open circles for current direction (oceanographic convention). The modeled currents follow the observations quite well, except during the event on days 336–338 when the strongest northward currents are observed. The model underestimates this northward flow.

4.2. Comparison With Sediment Concentrations at Moorings

First, we need to discuss the choice of two critical parameters used in the sediment transport model: critical bottom shear stress and settling velocity. It is not easy to measure the critical bottom shear stress $\tau_{b,cr}$ needed for sediment resuspension modeling in the lake. The only available direct field measurement of $\tau_{b,cr}$ for Lake Michigan was made using an in situ flume at a 65-m-deep station in southern Lake Michigan [*Hawley*, 1991], which showed that at that site, erosion oc-

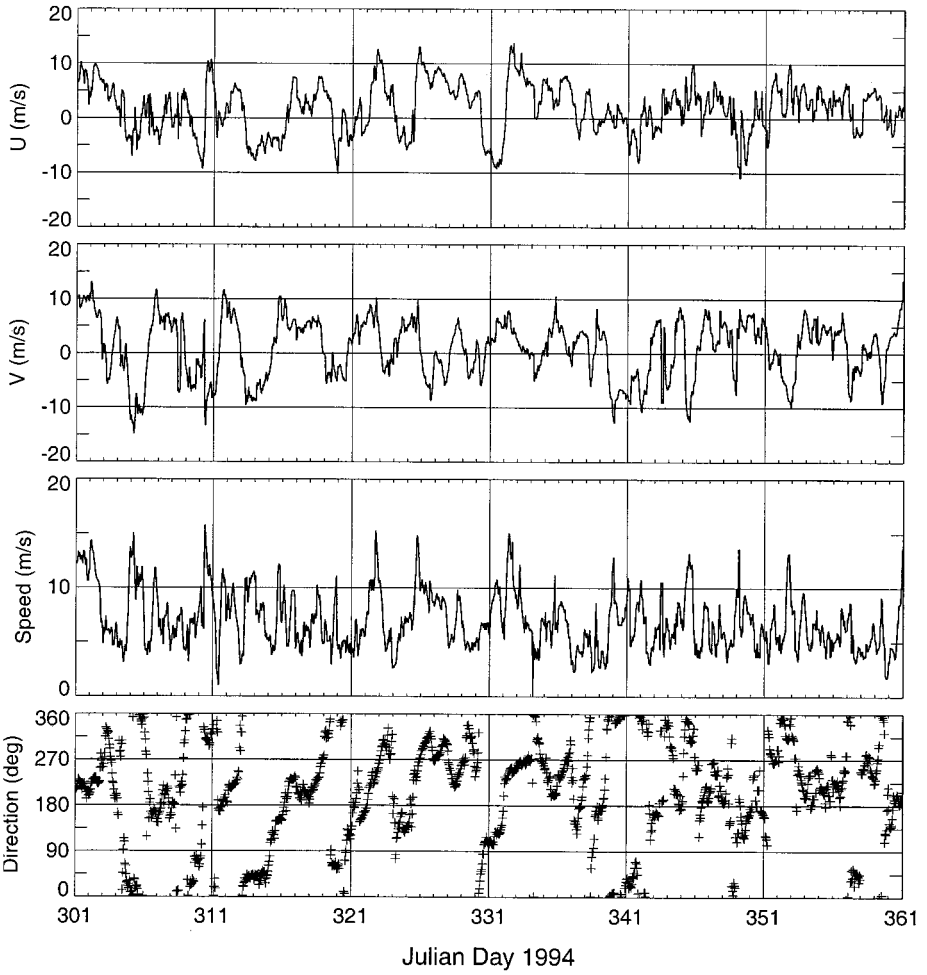

Figure 5. Winds at station 24 from Julian day 301–360 in 1994 (direction is meteorological convention).

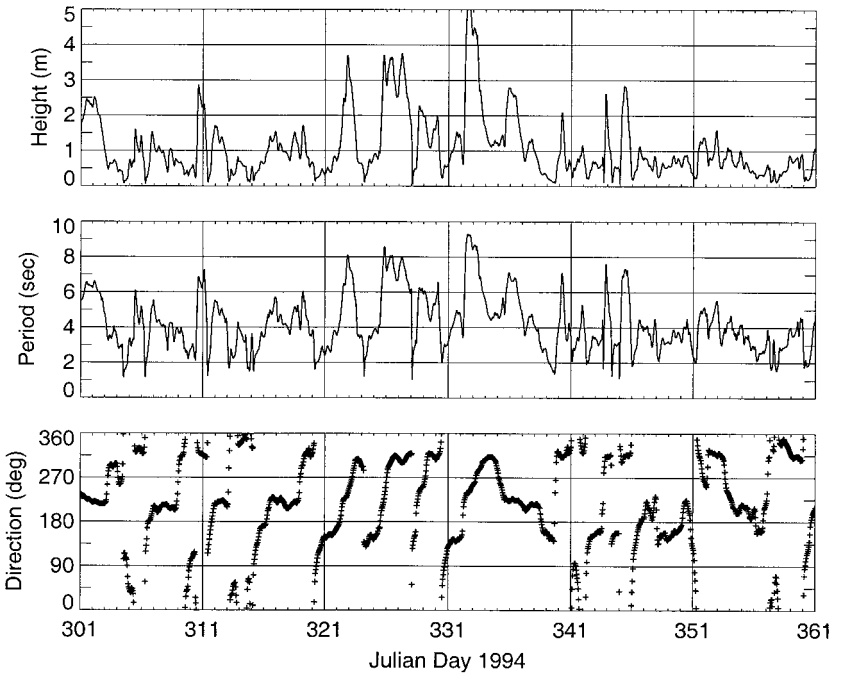

Figure 6. Modeled wave data at station 24 from Julian day 300–360 in 1994 (direction is meteorological convention).

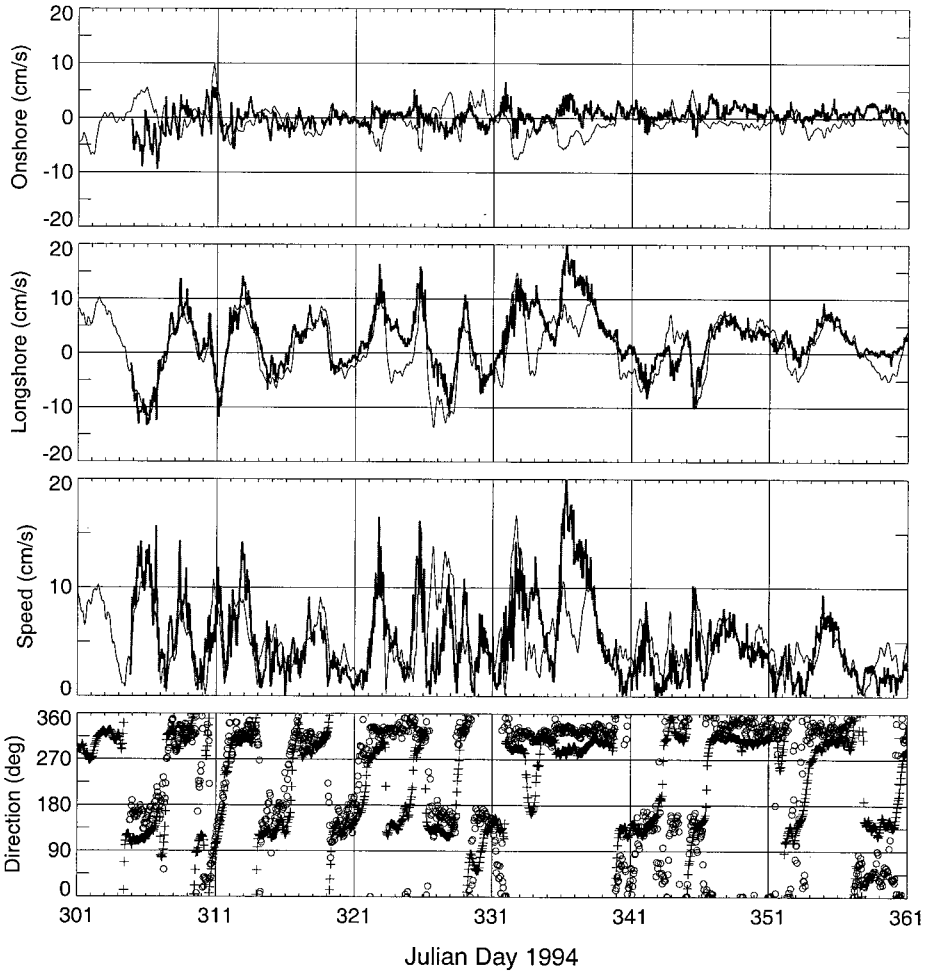

Figure 7. Modeled (thin, crosses) and observed (thick, open circles) bottom current at station 24 from Julian day 301 to 360 in 1994 (direction is oceanographic convention). The onshore and northward longshore currents are positive in the upper two panels.

curred at a shear stress from 0.009 to 0.134 N/m^2. Tests on material from the bottom of Lake Erie [*Fukuda and Lick*, 1980] showed that erosion began when the shear stress was of the order of 0.1–0.2 N/m^2. *Tsai and Lick* [1986] reported sediment entrainment of Lake St. Clair sediments at 0.25 N/m^2. In general, the critical shear stress is spatially variable and depends on many factors, including sediment grain size and composition. Dealing with the detailed spatial variability of critical shear stress is beyond the content of the present paper. Consistent with the single grain size used in the model, a uniform critical shear stress is assumed for this preliminary study. A series of tests were made using different values of critical shear stresses ranging from 0.05 to 0.2 N/m^2. This critical shear stress basically controls the magnitude of model results for suspended sediment concentration. The best fit between model results and field data was reached by using $\tau_c = 0.13$ N/m^2. As a result, in the present model study a value of 0.13 N/m^2 was adopted as the critical bottom stress. Most suspended particles in the water column are finer than the surficial bottom sediment [*Eadie and Lozano*, 1999]. A grain size of 30 μm is representative of these suspended particles. In addition, the main purpose of this study is to illustrate the hydrodynamic effect on sediment resuspension and transport. In this regard, simple sediment components will make the model result easier to understand. Thus in the model a uniform grain size of 30 μm with an unlimited sediment source on the bottom is used. Particle settling velocity was estimated from the ratio of mass flux trap data at station 19 to ambient suspended matter concentration. During the unstratified period, settling velocities in the water column are estimated at 5 m/d [*Eadie*, 1997], which is representative for the fine sediment particles during the sediment plume events. This settling velocity value is also a reasonable estimate for sediment particles of 30 μm in the Great Lakes. As a result, the above value of settling velocity was used in the sediment transport model.

The hydrodynamic and sediment transport models were calibrated and validated for a 60-day period from Julian days 301 to 360, 1994, during which hourly currents from the hydrodynamic model and the wave field from the wind wave model were used. The sediment transport model started running from zero initial condition, with a boundary condition of no sediment flux across lateral boundaries. The sediment measurement at stations 24 and 27 for high-turbidity events will be studied first because the data at these stations are more reliable and accurate than water intake data. The water intake data are only used to illustrate possible sources of model error and potential areas of model improvement. The capability of the sediment transport model to realistically

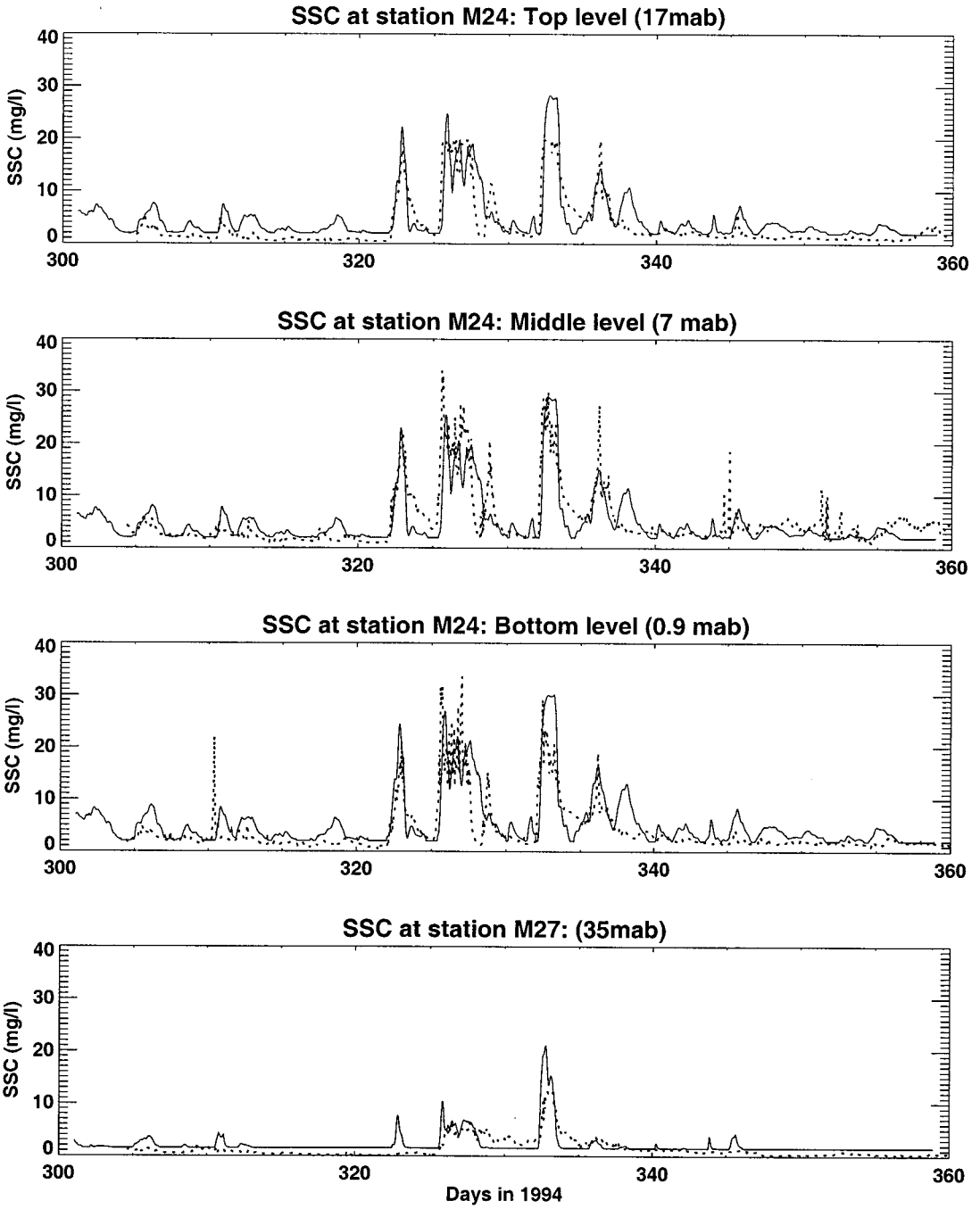

Figure 8. Suspended sediment concentration observations and predictions at stations 24 and 27 from Julian days 301 to 360 in 1994 (dashed line, observed data; solid line, model result).

simulate high concentration events in southern Lake Michigan is of critical importance because a high fraction of sediment is resuspended and transported during these relatively infrequent events.

Results of the sediment concentration simulation for Julian day 301–360, 1994 at station 24 (0.9 meters above bottom (mab), 7 mab, and 17 mab) and 27 (35 mab) are presented in Figure 8, along with the field measurement data. In the winter of 1994–1995 (Lake Michigan was practically ice-free in that mild winter), most observed sediment resuspension events occurred between Julian days 320 and 340. At some times the observed concentrations at 7 mab are greater than those at 0.9 mab at station 24. This is probably due to problems with the sensor calibrations [*Hawley and Lee*, 1999]. Generally, the model reproduced the high sediment concentration very well at both stations.

Examination of modeled waves (Figure 6) and bottom currents (Figure 7) at station 24 reveals that the current at this station is usually not strong enough ($<$0.2 m/s, which corresponds to shear stress of $\sim$0.1 N/m^2) to cause sediment resuspension. It showed that most major resuspensions were caused mainly by the combination of large waves and currents. The subpeak observed on Julian day 329 was probably the result of high sediment load discharge from the Grand River (Figure 9) moving northwest across station 24. Because no sediment loads

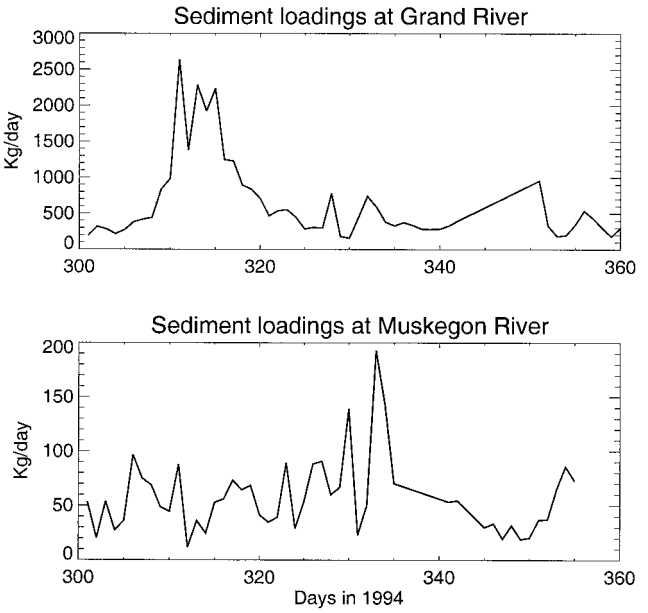

Figure 9. Daily sediment load discharge from Grand River and Muskegon River during Julian days 301–360 in 1994.

from lateral boundaries and tributaries were considered in the present model, the model cannot respond to this effect.

The discrepancy between model results and observations on Julian day 338 is probably the result of the unlimited sediment source assumption in the model. Owing to shallow water and frequent high wave activity, the area around station 24 forms one of the temporary, transient sediment reservoirs in the lake. The sediment material in these transient reservoirs is biogeochemically transformed within the lake, then redistributed throughout the year by a series of energetic events as suggested by *Eadie* [1997]. Large episodic events resuspend and transport most of these materials from temporary sinks to more permanent depositional basins, leaving less erodible materials for subsequent energetic events. To deal with this problem, a more realistic sediment mixture and sediment source distribution based on field surveys should be considered in the model. The concentration data at station 24 show more drop-off with height than the model results. This may also be related to the use of uniform grain size in the model.

At station 27 the resuspension is weaker due to deeper water and lower current speeds. Sediment concentration at this station varies only during the more energetic events. The model simulation reproduced the basic features of observed data at station 27.

The predicted surface concentration in the lake at 1600 UT on day 332, 1994, is given in Figure 10. It shows that sediment resuspension at that time mainly occurred in the southern part and along the east shore of the lake, which is consistent with the typical plume occurrence [*Eadie et al*., 1996]. There is a similarity in the 10–20 km width of the high sediment concentration area in both the model simulation and the observation from satellite imagery [*Eadie et al*., 1996; *Schwab et al*., 1999].

4.3. Comparison With Water Intake Data

Water turbidity data at five water intakes around southern Lake Michigan (Figure 11) from 1994–1995 were collected from water plant records. Water intake turbidity data were measured in National Turbidity Units (NTU), which are linearly related to the sediment concentration [*Hawley and Lee*, 1999]. Because the water intake position above the lake bottom, the distance between the intake and the water treatment plant where the turbidity measurement was made, and the water sample measurement process are different for each water intake and also because of our simple assumptions and the coarse grid size (5 km) used in the model, these water intake data were only used in a qualitative sense, with the main purpose to highlight potential problems and indicate possible direction for further model improvement.

Along the eastern side of the lake (Muskegon and St. Joseph), the model results generally follow the water intake turbidity pattern with several exceptions. At Muskegon the high-turbidity event after Julian day 310 was apparently due to a large sediment discharge from the Grand River (Figure 9) moving northward across this station. A similar explanation applies to the turbidity event between Julian days 312 and 315 at St. Joseph with high turbidity discharge from St. Joseph River. The discrepancy between model and observations at the St. Joseph station during Julian days 318–325 was probably caused by inaccurate wind wave predictions. The wave model was not able to predict high waves at this site during Julian days 318–325, though large waves were calculated to the north of this water intake station.

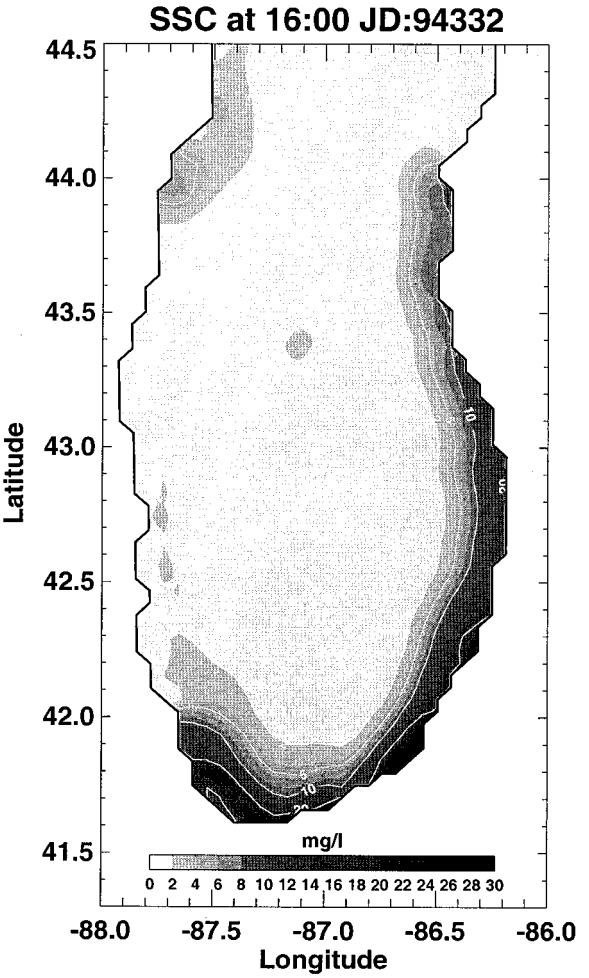

Figure 10. Predicted suspended sediment concentration at the surface at 1600 UT on day 332 in 1994 (the contour unit is in mg/L).

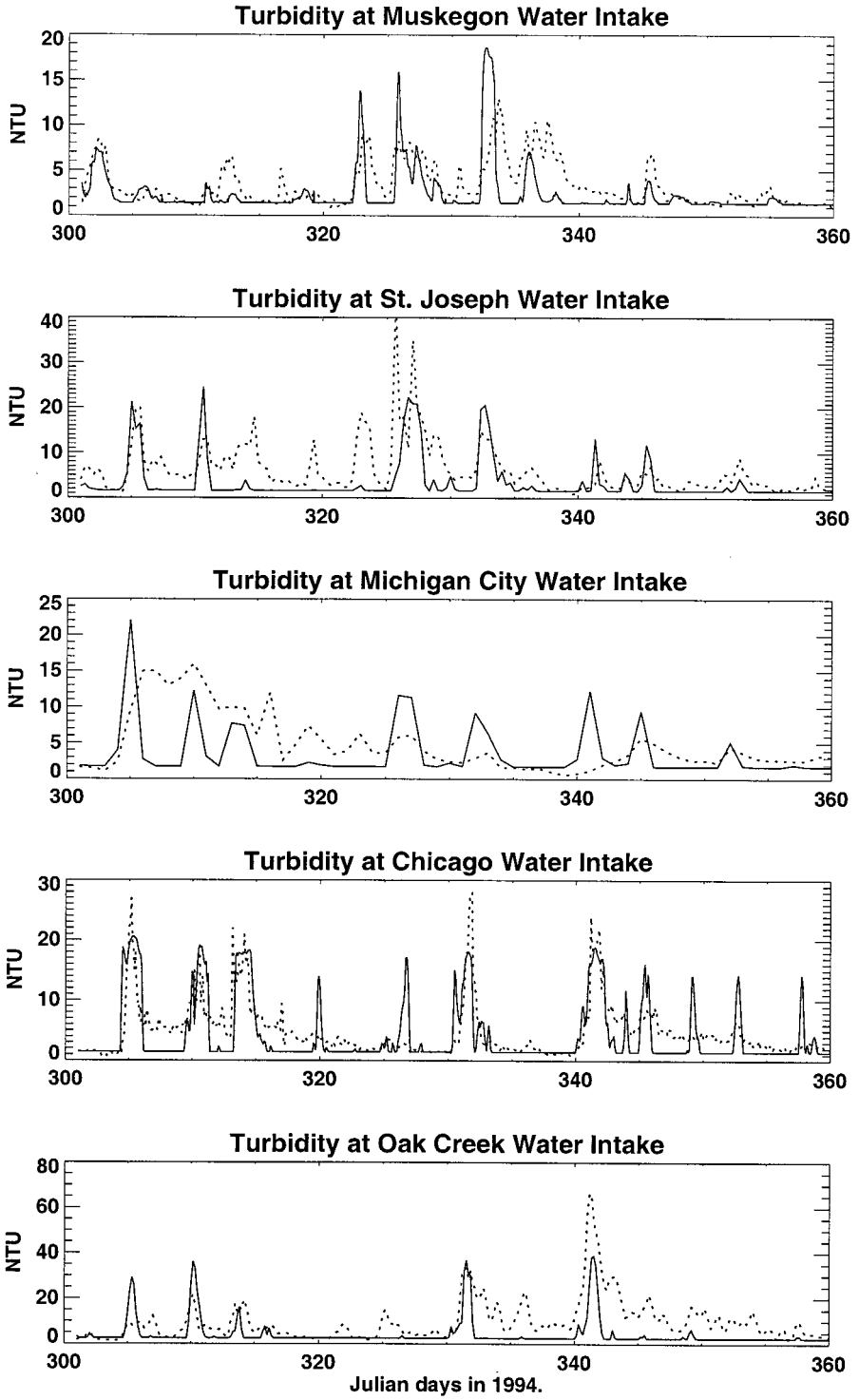

Figure 11. Water intake turbidities at five sites (dotted line, water intake data; solid line, model result).

In the southernmost part of the lake the model simulation can depict most major turbidity peaks (Michigan City and Chicago). However, the model has a general tendency to overestimate the turbidity data at many times after Julian day 320. This is believed to be a result of the unlimited sediment source assumption used in the model. In this region, the sediment particles are coarse (B. J. Eadie, personal communication, 1998) and the surface sediment layer is thinner, which limits the fine sediment sources available for resuspension. It is therefore not surprising to see the model systematically overestimate water turbidities after the initial resuspension events in this area.

Much of the western shoreline of Lake Michigan consists of steep bluffs, which are heavily eroded by wave action, temporal lake level changes, runoff, landsliding, and ice erosion [*Jibson et al.*, 1994; *Edil*, 1982; *Barnes et al.*, 1994]. The bluff erosion along this shoreline is one of the main contributions to lake sediment sources. It also results in local plume events in this region. Our model only calculates sediment resuspension from

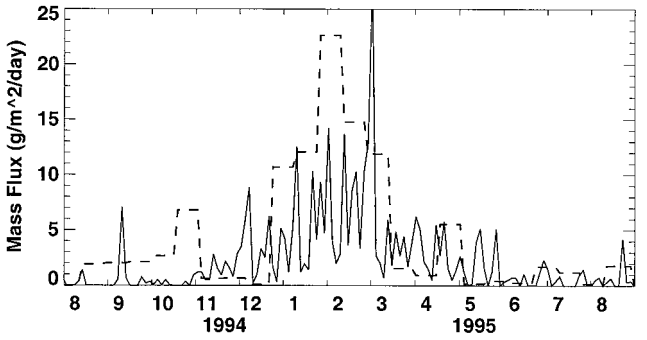

Figure 12. Settling mass fluxes at the trap station T at 30 m water depth (solid line, model result; dashed line, trap data sampling for 15-day intervals).

the bottom. No shoreline erosion effect has been taken into account. As a result, the turbidity increases due to coastline erosion were missed by the model, although some major resuspension events were still reproduced (Oak Creek in Figure 11).

These qualitative comparisons show that to improve the predictive ability of the sediment transport model in southern Lake Michigan, the following aspects should be addressed: a more realistic sediment mixture, rather than uniform grain size, should be used; an erosion function along the western shoreline should be incorporated into the model; available resuspendable sediment source distribution based on field surveys should be considered; and tributary sediment load discharge should be taken into account.

5. Two-Year (1994–1995) Model Simulations

5.1. Settling Mass Flux

A set of sequencing cylindrical sediment traps with an inner diameter of 20 cm and an aspect ratio of 8:1 above the collection funnel were deployed at station T (Figure 1) in 1994–1995. The trap station was located 21 km offshore in 56 m total water depth. The trap sampled sediment fluxes from August 1994 through August 1995 in 15-day intervals. In the deployment the trap was placed at middepth (30 m) to measure the settling mass fluxes. The trap data (Figure 12) shows a significant increase in mass collection during December 1994 to March 1995, with fluxes decreasing over other months. The trap collected ~85% of the annual input of particulate material to this region in a 10-week period centered in early February 1995. There were two other smaller mass flux events in late October 1994 and April 1995. On the basis of the 1994–1995 model prediction the settling sediment fluxes at the same height as the trap location were calculated and compared with the observed trap data. The model results successfully reproduced an increase in mass flux in the winter and early spring, coinciding with the trap observations. Because only one single grain size of 30 μm was considered in the model, there is a systematic magnitude difference between trap observation and the model result. The trap collection increase in October 1994 resulted from the rise in the inorganic carbon content of the trap material during the annual calcite precipitation (whiting) event [*Strong and Eadie*, 1978]. At that time, about half of the trap material was calcium carbonate produced mainly by strong biological activity in the water column [*Robbins and Eadie*, 1991]. Because the model could not account for this effect, the October trap event is not seen in the model results. The modeled higher peak in later February 1995 is probably caused by the unlimited sediment source assumption used in the model.

5.2. Erosion and Deposition

Foster and Colman [1992] mapped the long-term accumulation and thickness distribution of Holocene lake sediment based on the sediment core data (Figure 13). The area of lake sediment deposition is restricted to eastern side, while most erosions can be found in the western part. The highest deposition area locates close to eastern shore with the maximum sediment accumulation thickness up to 14 m. Results of sediment resuspension and transport simulations allow us to examine the sediment erosion and deposition zones in southern Lake Michigan. A complete study of the lake morphodynamics is beyond the content of this work. In addition, the bed load transport, shoreline erosion, and tributary sediment discharge, which have not been considered by this study, all have a significant contribution to the erosion-deposition process. In this section a simple estimation of bottom erosion and deposition is made based on the 2-year (1994–1995) sediment transport results, with the purpose of highlighting the hydrodynamical effects on sediment redistribution in the lake. None of the model parameters were adjusted during this 2-year model simulation. During the course of model simulation the sediment layer thickness changes with bottom sediment resuspension and/or settling down from the water column. The vertical sediment fluxes at the fluid-sediment interface were calculated using (15). The erosion and deposition were determined by comparing the final sediment layer thickness with the initial thickness. The net change in bed thickness resulting from the 1994–1995 simulation is given in Figure 14. The general feature is that net erosion occurs along the shoreline and the deposition occurs offshore. The largest net deposition occurs offshore in the southeastern part of the lake, as well as offshore of the western and eastern sides around the lake ridge area (upper part in Figure 14). The greatest erosion occurs along the shores in the southwestern and southeastern parts of the lake with the largest erosion in sediment thickness over 6 mm. Relatively weak erosion also occurs in deep waters in the ridge area and the midwestern part of the central lake basin. Overall, the modeled deposition pattern during this 2-year period is similar to the long-term sediment accumulation map shown in Figure 13. Both show an asymmetric pattern of sediment deposition, with maximum deposition occurring mainly in the eastern side of the lake in water depth of 50–100 m.

Although uniform grain size and unlimited sediment sources are assumed in the model, the results do illustrate the hydrodynamical effect on sediment redistribution in southern Lake Michigan. With the qualitative agreement between the sediment accumulation survey (Figure 13) and the model simulation result (Figure 14), the preliminary model predictions are considered to be successful. Given that the bottom sediment dry bulk density is 1450 kg/m^3, the estimated total resuspended mass in 1994–1995 in southern Lake Michigan was 1.24×10^{10} kg, which gives the estimated annual resuspension of about 6.2×10^9 kg. During the high resuspension event between Julian days 331 and 335, 1994, the calculated resuspension was 0.91×10^9 kg. This value is comparable to the total mass of material of 1.03×10^9 kg in the 1996 April sediment plume event [*Eadie et al.*, 1996]. The resuspension in the high-turbidity period during Julian days 320–340, 1994, was $1.89 \times$

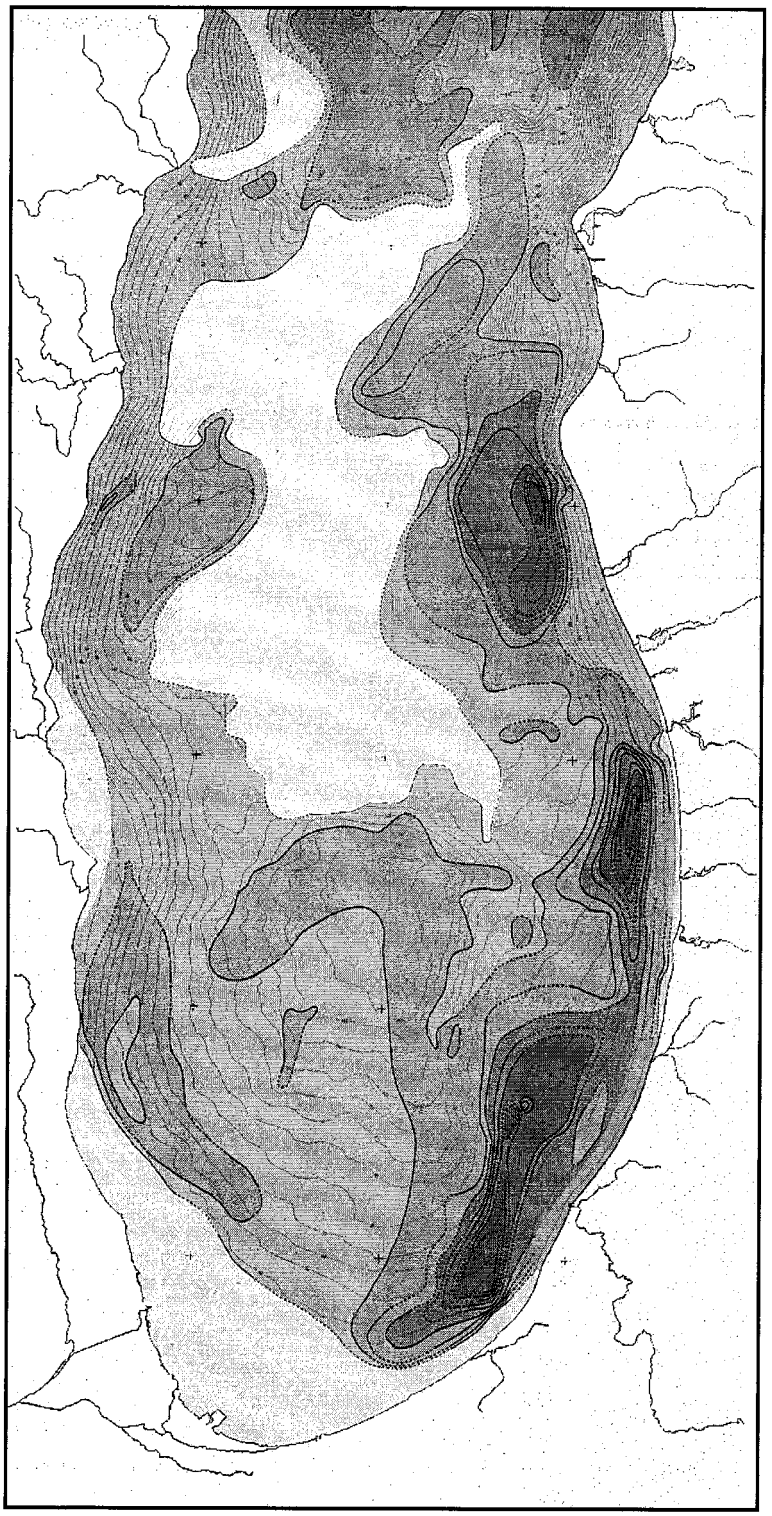

Figure 13. Sediment accumulation patterns in southern Lake Michigan as measured by post-glacial sediment [from *Foster and Colman*, 1992]. The five ranges of sediment thickness depicted in the map are (from lightest to darkest): 1–2 m, 2–6 m, 6–10 m, 10–14 m, and >14 m.

10^9 kg, ~30% of the annual resuspension amount. Given the fact that most of the sediment resuspension events occur during winter and spring, this seems like a reasonable prediction, which encourages further model improvements and applications. It is believed that circulation and wind waves play an important role in nearshore-offshore sediment transport. The inclusion of wind waves in the sediment entrainment bottom shear stress is an essential requirement, especially in shallow coastal waters, and it is also responsible for the accurate calculation of nearshore sediment resuspension (erosion).

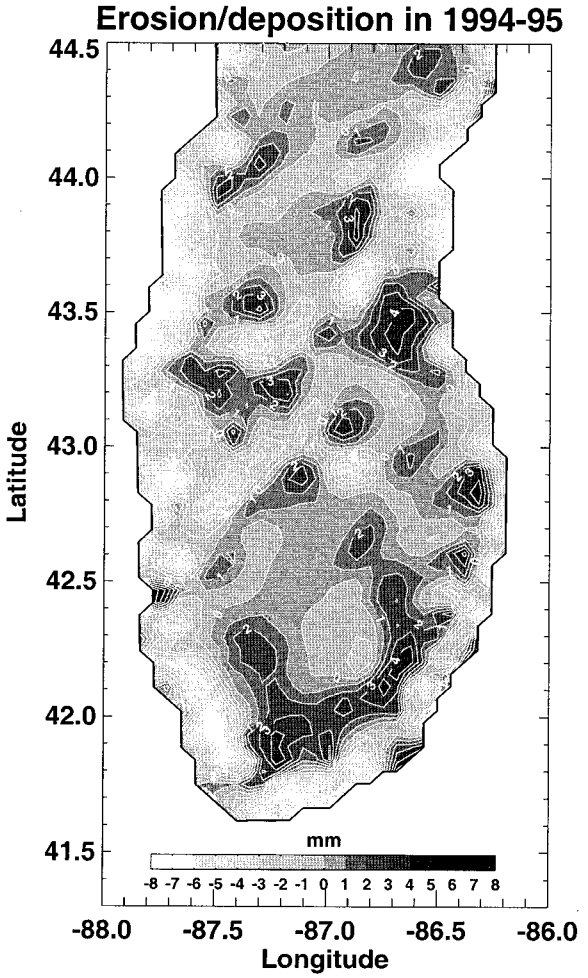

Figure 14. Net sediment thickness changes in southern Lake Michigan after the 1994–1995 model simulation. The contours are in mm, positive values (dark areas) represent deposition, and negative values (light areas) represent erosion.

6. Conclusions

The quasi-3-D sediment transport model was integrated with hydrodynamic circulation and wind wave models to study the resuspension dynamics in southern Lake Michigan. Wave-current interaction, a nonlinear bottom shear stresses, and turbulent eddy coefficient changes due to wave-current coexistence have been included. The sediment entrainment and resuspension were parameterized and calibrated by laboratory data and field studies in the lake. Wave-current interaction was found to play an important role in the bottom shear stresses and therefore in the sediment resuspension and transport processes.

The model successfully predicted the major sediment resuspension events at two field stations in November–December 1994. The capability of the sediment transport model to realistically simulate high concentration events in southern Lake Michigan is of critical importance because a large fraction of sediment is resuspended and transported during these relatively infrequent events. The predicted sediment plume occurrence was consistent with our current knowledge based on the satellite observations. The difference between the model results and water intake data reveals the importance of sediment source functions (shoreline erosion, river discharge and bottom sediment availability) at these nearshore/onshore locations. A sediment erosion and deposition simulation was performed using the 1994–1995 hydrodynamic model results. It predicted the sediment erosion and accumulation areas reasonably well. The model also reproduced the increase in mass flux in winter and early spring, consistent with the trap measurement data.

Although the modeling framework used in the present study has proven effective, the model does possess some limitations. Several areas have been identified that require further laboratory and field research and improvement of the model. A sediment mixture based on the field survey of grain size distribution should be included; sediment source input from shoreline erosion, tributary discharge, and bottom sediment availability function need to be included; cohesive flocculation should also be taken into account. More field data on the settling velocity, critical bottom shear stresses, and sediment concentration under various conditions need to be collected.

Despite the simple assumptions and the limitations of the sediment transport model, it illustrates the importance of hydrodynamic effects on sediment resuspension and transport in southern Lake Michigan and leads to better understanding of the complicated processes involving interaction among sediment, topography, circulation, and wind waves. Therefore the modeling system developed here presents a useful tool for further sediment transport studies in the Great Lakes.

Appendix: Asymptotic Quasi-3-D Solution of Convection-Diffusion Equation

In this section the convection-diffusion equation for concentration distribution (1) is solved with an asymptotic quasi-3-D solution as first introduced by *Galappatti* [1983] in his 2DV model for a steady uniform current.

A1. Scale Analysis and Fundamental Assumptions

In (1), let the characteristic scale for time, water depth, horizontal dimension, horizontal flow velocity, vertical velocity, horizontal diffusion coefficient, and vertical diffusion coefficient be denoted by T, H, L, U, UH/L, E_h, and E, respectively. Then (1) can be rewritten in dimensionless form as

$$\frac{H}{w_s T}\frac{\partial c}{\partial t'} + \frac{HU}{Lw_s}\left(\frac{\partial c}{\partial x'} + \frac{\partial c}{\partial y'} + \frac{\partial c}{\partial z'}\right) - \frac{\partial c}{\partial z'} = \frac{E_h H}{L^2 w_s}\left[\frac{\partial}{\partial x'}\left(E'\frac{\partial c}{\partial x'}\right) + \frac{\partial}{\partial y'}\left(E'\frac{\partial c}{\partial y'}\right)\right] + \frac{E}{Hw_s}\frac{\partial}{\partial z'}\left(E'\frac{\partial c}{\partial z'}\right) \tag{20}$$

where all quantities marked with superscript prime have been made dimensionless using the corresponding characteristic scale.

The order of magnitude of E is proportional to $\kappa u_* H$, where κ is von Karman constant and u_* is the bed shear velocity, and thus

$$O\left(\frac{E}{Hw_s}\right) \sim O\left(\kappa\frac{u_*}{w_s}\right) \sim O(1) \tag{21}$$

where O represents the order of magnitude. The following further assumptions are made:

$$O(H/w_sT) = O(\delta) < 1$$
$$O(HU/Lw_s) = O(\delta) < 1 \qquad (22)$$
$$O(E_hH/L^2w_s) = O(\delta) < 1$$

with δ is a first-order small variable.

The assumptions in (22) are valid for most coastal regions. For example, in Lake Michigan, if $H = 100$ m, $T = 10$ days, $w_s = 10^{-3}$ m/s, $U = 0.4$ m/s, $L = 200$ km, and $E_h = 1.0$ m^2/s, then $H/w_sT = 0.1$, $HU/Lw_s = 0.2$, and $E_hH/L^2w_s = 2.5 \times 10^{-6}$.

These assumptions imply that the main physical mechanism for concentration distribution is the balance between diffusion and settling in the vertical direction. This means that the concentration field does not deviate too much from the equilibrium state. On the basis of these assumptions, an asymptotic solution for concentration may be established as follows.

A2. Asymptotic Solutions

An asymptotic solution for (1) can be expressed as

$$c(x, y, z, t) = \sum_{i=0}^{n} c_i(x, y, z, t) + O(\delta^{n+1}), \qquad (23)$$

where $c_i(x, y, z, t)$ is the ith-order solution of concentration $c(x, y, z, t)$, $\delta(\ll 1)$ is a small residual magnitude, and O represents the magnitude order.

Substituting (23) into (1) and combining with the above assumption, c_i ($i = 0, 1, 2, \ldots$) satisfy the following equations:

$$w_s \frac{\partial c_0}{\partial z} + \frac{\partial}{\partial z}\left(\varepsilon_z \frac{\partial c_0}{\partial z}\right) = 0 \qquad (24)$$

$$w_s \frac{\partial c_i}{\partial z} + \frac{\partial}{\partial z}\left(\varepsilon_z \frac{\partial c_i}{\partial z}\right) = \frac{Dc_{i-1}}{Dt} - \frac{\partial}{\partial x}\left(\varepsilon_x \frac{\partial c_{i-1}}{\partial x}\right) - \frac{\partial}{\partial y}\left(\varepsilon_y \frac{\partial c_{i-1}}{\partial y}\right), \quad (i = 1, 2, \ldots), \qquad (25)$$

respectively, where

$$\frac{D}{Dt} = \frac{\partial}{\partial t} + u\frac{\partial}{\partial x} + v\frac{\partial}{\partial y} + w\frac{\partial}{\partial z}. \qquad (26)$$

In order to deal with irregular bathymetry, it is convenient to introduce a new coordinate ζ in vertical direction as

$$\zeta = \frac{z - a}{h} \qquad (27)$$

where h is the total water depth and a is the reference fluid-sediment interface level where the sediment particles start to suspend. It is assumed that $h \gg a$. Using this transformation, the lake surface and the reference bottom have been changed into regular shapes corresponding to $\zeta = 1$ and $\zeta = 0$, respectively.

Denote depth-averaged quantities with overbars, and let the velocity profile components be described by

$$p_x = u/\bar{u}, \qquad p_y = v/\bar{v}. \qquad (28)$$

Once horizontal velocities are given, the vertical velocity component w can be obtained from the flow continuity equation:

$$\frac{\partial u}{\partial x} + \frac{\partial v}{\partial y} + \frac{\partial w}{\partial z} = 0. \qquad (29)$$

Thus

$$w = \frac{\partial}{\partial x}[\bar{u}hP_x(\zeta)] + \frac{\partial}{\partial y}[\bar{v}hP_y(\zeta)], \qquad (30)$$

where

$$P_{x,y}(\zeta) = \int_{\zeta}^{0} p_{x,y}(\zeta)\, d\zeta. \qquad (31)$$

Therefore, (24) and (25) can be rewritten as

$$\mathcal{R}[c_0] = 0 \qquad (32)$$

$$\mathcal{R}[c_i] = \left(\frac{h}{w_s}\frac{\partial}{\partial t} + \frac{\bar{u}h}{w_s}p_x(\zeta)\frac{\partial}{\partial x} + \frac{\bar{v}h}{w_s}p_y(\zeta)\frac{\partial}{\partial y} + \frac{w}{w_s}\frac{\partial}{\partial \zeta}\right)c_{i-1} - \frac{h}{w_s}\frac{\partial}{\partial x}\left(\varepsilon_x\frac{\partial c_{i-1}}{\partial x}\right) - \frac{h}{w_s}\frac{\partial}{\partial y}\left(\varepsilon_y\frac{\partial c_{i-1}}{\partial y}\right) \qquad (33)$$

where $\mathcal{R}$ is a second-order derivative operator:

$$\mathcal{R}[\quad] = \frac{\partial}{\partial \zeta} + \frac{\partial}{\partial \zeta}\left(\varepsilon'\frac{\partial}{\partial \zeta}\right) \qquad (34)$$

with

$$\varepsilon' = \varepsilon_z/w_sh.$$

Furthermore, it is assumed that only the zeroth-order solution (equilibrium concentration) contributes to the depth-averaged concentration. Because (32) is a differential equation in ζ only, it is possible to write the zeroth-order solution in the following form:

$$c_0(x, y, \zeta, t) = a_{11}(\zeta, t)\bar{c}(x, y, t), \qquad (35)$$

and the following relations can be obtained:

$$\mathcal{R}[a_{11}(\zeta)] = 0, \qquad \overline{a_{11}(\zeta)} = 1. \qquad (36)$$

At the water surface, if there is no vertical net sediment flux, the following boundary condition then satisfies

$$\left(a_{11}(\zeta) + \varepsilon'\frac{\partial a_{11}}{\partial \zeta}\right)\Big|_{\zeta=1} = 0. \qquad (37)$$

From (36) and (37) the vertical function $a_{11}(\zeta)$ can be found.

A2.1. First-order approximation. If the flow variation is gradual, settling velocity w_s is independent of water depth, and the equilibrium concentration profile changes slowly, the first-order solution ($i = 1$) is then reduced to

$$\mathcal{R}[c_1] = \frac{h}{w_s}a_{11}(\zeta)\frac{\partial \bar{c}}{\partial t} + \frac{\bar{u}h}{w_s}p_x(\zeta)a_{11}(\zeta)\frac{\partial \bar{c}}{\partial x} + \frac{\bar{v}h}{w_s}p_y(\zeta)a_{11}(\zeta)\frac{\partial \bar{c}}{\partial y} - \frac{h}{w_s}a_{11}(\zeta)\frac{\partial}{\partial x}\left(\varepsilon_x\frac{\partial \bar{c}}{\partial x}\right) - \frac{h}{w_s}a_{11}(\zeta)\frac{\partial}{\partial y}\left(\varepsilon_y\frac{\partial \bar{c}}{\partial y}\right) + \frac{h}{w_s}\frac{\partial a_{11}(\zeta)}{\partial \zeta} \cdot \left(P_x(\zeta)\frac{\partial \bar{u}}{\partial x} + P_y(\zeta)\frac{\partial \bar{v}}{\partial y}\right)\bar{c}. \qquad (38)$$

Because this equation is a second-order differential equation in ζ only, it is possible to write the solution in the form as follows:

$$c_1(x, y, \zeta, t) = a_{21}(\zeta)\frac{h}{w_s}\frac{\partial \bar{c}}{\partial t} + a_{22}(\zeta)\frac{\bar{u}h}{w_s}\frac{\partial \bar{c}}{\partial x} + a_{23}(\zeta)\frac{\bar{v}h}{w_s}\frac{\partial \bar{c}}{\partial y} - a_{21}(\zeta)\frac{h}{w_s}\frac{\partial}{\partial x}\left(\varepsilon_x\frac{\partial \bar{c}}{\partial x}\right) - a_{21}(\zeta)\frac{h}{w_s}\frac{\partial}{\partial y}\left(\varepsilon_y\frac{\partial \bar{c}}{\partial y}\right) + \frac{h}{w_s}\left(a_{24}(\zeta)\frac{\partial \bar{u}}{\partial x} + a_{25}(\zeta)\frac{\partial \bar{v}}{\partial y}\right)\bar{c}, \quad (39)$$

where $a_{2j}(\zeta)$ $(j = 1, 2, 3, 4, 5)$ satisfy

$$\mathcal{R}[a_{21}(\zeta)] = a_{11}(\zeta)$$
$$\mathcal{R}[a_{22}(\zeta); a_{23}(\zeta)] = [a_{11}(\zeta)p_x(\zeta); a_{11}(\zeta)p_y(\zeta)]$$
$$\mathcal{R}[a_{24}(\zeta); a_{25}(\zeta)] = \left(\frac{\partial a_{11}(\zeta)}{\partial \zeta}P_x(\zeta); \frac{\partial a_{11}(\zeta)}{\partial \zeta}P_y(\zeta)\right). \quad (40)$$

With the definition of (36), $a_{2j}(\zeta)$ $(j = 1, 2, 3, 4, 5)$ should meet the conditions:

$$\int_0^1 a_{2j}(\zeta)\, d\zeta = 0 \qquad (j = 1, 2, 3, 4, 5). \quad (41)$$

Similarly, the no flux surface boundary condition must be satisfied for the first-order term solution; thus we have

$$\left(a_{2j}(\zeta) + \varepsilon'(\zeta)\frac{\partial a_{2j}(\zeta)}{\partial \zeta}\right)\Big|_{\zeta=1} = 0 \qquad (j = 1, 2, 3, 4, 5). \quad (42)$$

Therefore the vertical profile functions $a_{2j}(\zeta)$ $(j = 1, 2, 3, 4, 5)$ can be obtained by solving differential equations (40), with conditions (41) and (42), respectively. It is clear that $a_{11}(\zeta)$ represents the equilibrium concentration profile, while $a_{2j}(\zeta)$ $(j = 1, 2, 3, 4, 5)$ gives the modifications to this equilibrium concentration profile. The settling velocity, diffusion coefficient, and velocity profiles determine the vertical concentration structure.

The higher-order solutions $(c_2, c_3, \ldots, c_n)$ can be obtained in the same way by using the calculated lower-order solutions. However, the contributions from these higher-order solutions are relatively small and decrease rapidly [*Lou*, 1995]. For most of the hydrodynamic conditions the first-order solutions can often give reasonable results.

After the vertical functions $(a_{ij}, i = 1, 2; j = 1, 2, 3, 4, 5)$ are solved, the asymptotic solution for concentration with first order accuracy can be expressed as

$$c(x, y, \zeta, t) = \left\{a_{11}(\zeta) + \frac{h}{w_s}\left(a_{24}(\zeta)\frac{\partial \bar{u}}{\partial x} + a_{25}(\zeta)\frac{\partial \bar{v}}{\partial y}\right)\right\}\bar{c} + a_{21}(\zeta)\frac{h}{w_s}\frac{\partial \bar{c}}{\partial t} - a_{21}(\zeta)\frac{h}{w_s}\frac{\partial}{\partial x}\left(\varepsilon_x\frac{\partial \bar{c}}{\partial x}\right) - a_{21}(\zeta)\frac{h}{w_s}\frac{\partial}{\partial y}\left(\varepsilon_y\frac{\partial \bar{c}}{\partial y}\right) + a_{22}(\zeta)\frac{\bar{u}h}{w_s}\frac{\partial \bar{c}}{\partial x} + a_{23}(\zeta)\frac{\bar{v}h}{w_s}\frac{\partial \bar{c}}{\partial y}. \quad (43)$$

The above concentration solution satisfies the convection-diffusion equation (1) and the surface boundary condition. The vertical profile functions $a_{ij}(\zeta)$ can be determined in advance if the velocity profile $p_{x,y}(\zeta)$ and the vertical diffusion coefficient ε_z are known.

Using (43), the bottom boundary condition at the reference level $z = a$ $(\zeta = 0)$ can be reformulated in terms of the depth-averaged concentration as

$$c(x, y, 0, t) = \left\{\gamma_{11} + \frac{h}{w_s}\left(\gamma_{24}\frac{\partial \bar{u}}{\partial x} + \gamma_{25}\frac{\partial \bar{v}}{\partial y}\right)\right\}\bar{c} + \gamma_{21}\frac{h}{w_s}\frac{\partial \bar{c}}{\partial t} - \gamma_{21}\frac{h}{w_s}\frac{\partial}{\partial x}\left(\varepsilon_x\frac{\partial \bar{c}}{\partial x}\right) - \gamma_{21}\frac{h}{w_s}\frac{\partial}{\partial y}\left(\varepsilon_y\frac{\partial \bar{c}}{\partial y}\right) + \gamma_{22}\frac{\bar{u}h}{w_s}\frac{\partial \bar{c}}{\partial x} + \gamma_{23}\frac{\bar{v}h}{w_s}\frac{\partial \bar{c}}{\partial y}, \quad (44)$$

where $\gamma_{ij} = a_{ij}(\zeta = 0)$.

Equation (44) is a differential equation for the unknown depth-averaged concentration $\bar{c}(x, y, t)$ with constant coefficients which can be determined in advance if the velocity profile and vertical turbulent diffusion coefficient are known. Once $\bar{c}(x, y, t)$ has been determined, by solving this equation with proper conditions at the upstream boundary and initial condition, the three-dimensional concentration distribution can be obtained from (43). Therefore the 3-D convection-diffusion concentration equation has been reduced to a quasi-3-D model: a two-dimensional horizontal model for depth-averaged concentration with the corresponding vertical profiles determined by the asymptotic solution scheme.

A2.2. Sediment transport rate. The suspended sediment transport rate in x and y directions are defined as

$$S_x = \int_a^h \left(uc - \varepsilon_x\frac{\partial c}{\partial x}\right) dz = h\int_0^1 \left(uc - \varepsilon_x\frac{\partial c}{\partial x}\right) d\zeta \quad (45)$$

$$S_y = \int_a^h \left(vc - \varepsilon_y\frac{\partial c}{\partial y}\right) dz = h\int_0^1 \left(vc - \varepsilon_y\frac{\partial c}{\partial y}\right) d\zeta. \quad (46)$$

Substituting (43) into (45) and (46), the sediment transport rate with first-order accuracy can be obtained by

$$S_x = h\bar{u}\left\{\left[\alpha_{11} + \frac{h}{w_s}\left(\alpha_{24}\frac{\partial \bar{u}}{\partial x} + \alpha_{25}\frac{\partial \bar{v}}{\partial y}\right)\right]\bar{c} + \frac{h}{w_s}\cdot\left(\alpha_{22}\bar{u}\frac{\partial \bar{c}}{\partial x} + \alpha_{23}\bar{v}\frac{\partial \bar{c}}{\partial y}\right) + \alpha_{21}\frac{h}{w_s}\frac{\partial \bar{c}}{\partial t} - \alpha_{21}\frac{h}{w_s}\cdot\left[\frac{\partial}{\partial x}\left(\varepsilon_x\frac{\partial \bar{c}}{\partial x}\right) + \frac{\partial}{\partial y}\left(\varepsilon_y\frac{\partial \bar{c}}{\partial y}\right)\right]\right\} - h\varepsilon_x\frac{\partial \bar{c}}{\partial x} \quad (47)$$

$$S_y = h\bar{v}\left\{\left[\alpha_{11} + \frac{h}{w_s}\left(\alpha_{24}\frac{\partial \bar{u}}{\partial x} + \alpha_{25}\frac{\partial \bar{v}}{\partial y}\right)\right]\bar{c} + \frac{h}{w_s}\cdot\left(\alpha_{22}\bar{u}\frac{\partial \bar{c}}{\partial x} + \alpha_{23}\bar{v}\frac{\partial \bar{c}}{\partial y}\right) + \alpha_{21}\frac{h}{w_s}\frac{\partial \bar{c}}{\partial t} - \alpha_{21}\frac{h}{w_s}\cdot\left[\frac{\partial}{\partial x}\left(\varepsilon_x\frac{\partial \bar{c}}{\partial x}\right) + \frac{\partial}{\partial y}\left(\varepsilon_y\frac{\partial \bar{c}}{\partial y}\right)\right]\right\} - h\varepsilon_y\frac{\partial \bar{c}}{\partial y}, \quad (48)$$

where

$$\alpha_{ij} = \int_0^1 a_{ij}(\zeta)p(\zeta)\, d\zeta. \quad (49)$$

Acknowledgments. The authors wish to express their appreciation to the following people who were helpful either during collecting and analysis of data, discussion, or other aspects of the work described herein: Brain Eadie, Douglas Endicott, John Robbins, and Rick Towler. We also thank two anonymous reviewers for their critical comments and suggestions that improved the manuscript. This work was performed while JL held a National Research Council, NOAA/GLERL Research Associateship. D.J.S., D.B., and N.H. were partially supported by the EPA Lake Michigan Mass Balance Study project. This is NOAA/GLERL contribution 1121.

References

Ayers, J. C., A dynamic height method for the determination of currents in deep lakes, *Limnol. Oceanogr*., *1*, 150–161, 1956.

Barnes, P. W., E. W. Kempema, E. Reimnitz, and M. McCormick, The influence of ice on southern Lake Michigan coastal erosion, *J. Great Lakes Res*., *20*, 179–195, 1994.

Beletsky, D., and D. J. Schwab, Modeling thermal structure and circulation in Lake Michigan, in *Estuarine and Coastal Modeling: Proceedings of 5th International Conference*, edited by M. L. Spaulding and A. F. Blumberg, pp. 511–522, Am. Soc. of Civ. Eng., Reston, Va., 1998.

Bennett, J. R., On the dynamics of wind-driven lake currents, *J. Phys. Oceanogr*., *4*, 400–414, 1974.

Bennett, J. R., Another explanation of the observed cyclonic circulation of large lakes, *Limnol. Oceanogr*., *20*, 108–110, 1975.

Blumberg, A. F., and G. L. Mellor, A description of a three-dimensional coastal ocean circulation model, in *Three-Dimensional Coastal Ocean Models*, *Coastal Estuarine Sci*., vol. 4, edited by N. S. Heaps, pp. 1–16, AGU, Washington, D. C., 1987.

Bosman, J., Concentration measurements under oscillatory motion, *Rep. M1695-II*, Delft Hydraul. Lab., Delft, Netherlands, 1982.

Brooks, A. S., and D. N. Edgington, Biogeochemical control of phosphorus cycling and primary production in Lake Michigan, *Limnol. Oceanogr*., *39*, 962–968, 1994.

Colman, S. M., and D. S. Foster, A sediment budget for southern Lake Michigan: Source and sink models for different time intervals, *J. Great Lakes Res*., *20*, 215–228, 1994.

Csanady, G. T., Lateral momentum flux in boundary currents, *J. Phys. Oceanogr*., *5*, 705–717, 1975.

Eadie, B. J., Probing particle processes in Lake Michigan using sediment traps, *Water Air Soil Pollut*., *99*, 133–139, 1997.

Eadie, B. J., and S. Lozano, Grain size distribution of the surface sediments collected during the Lake Michigan Mass Balance and Environmental Mapping and Assessment Programs, *NOAA Tech. Memo. ERL GLERL-111*, 42 pp., Great Lakes Environ. Res. Lab., Ann Arbor, Mich., 1999.

Eadie, B. J., and J. A. Robbins, The role of particulate matter in the movement of contaminants in the Great Lakes, in *Sources and Fates of Aquatic Pollutants*, *ACS Adv. Chem. Ser*., vol. 216, edited by R. Hites and S. Eisenreich, pp. 319–364, Am. Chem. Soc., Washington, D. C., 1987.

Eadie, B. J., R. L. Chambers, W. S. Gardner, and G. L. Bell, Sediment trap studies in Lake Michigan: Resuspension and chemical fluxes in the southern basin, *J. Great Lakes Res*., *10*, 307–321, 1984.

Eadie, B. J., H. A. Vanderploeg, J. A. Robbins, and G. L. Bell, Significance of sediment resuspension and particle settling, in *Large Lakes*, edited by M. M. Tilzer and C. Serruya, pp. 196–209, Springer-Verlag, New York, 1990.

Eadie, B. J., B. McKee, M. B. Lansing, J. A. Robbins, S. Metz, and J. H. Trefry, Nutrient enhanced coastal ocean productivity recorded in sediments from the Louisiana shelf, *Estuaries*, *17*, 754–766, 1994.

Eadie, B. J., et al., Recurrent coastal plume in southern Lake Michigan, *Eos Trans. AGU*, *77*, 337–338, 1996.

Edil, T. B., Causes and mechanics of coastal bluff recession in the Great Lakes, paper presented at Bluff Slumping Workshop, Mich. Sea Grant Program, Ann Arbor, Mich., 1982.

Foster, D. S., and S. M. Colman, Thickness and distribution of postglacial deposits in Lake Michigan, *U.S. Geol. Surv. Misc. Invest. Map*, *MI-2202*, 1992.

Fukuda, M., and W. Lick, The entrainment of cohesive sediments in freshwater, *J. Geophys. Res*., *85*, 2813–2824, 1980.

Gailani, J., C. K. Ziegler, and W. Lick, Transport of suspended solids in the Lower Fox River, *J. Great Lakes Res*., *17*, 479–494, 1991.

Galappatti, R., A depth-integrated model for suspended sediment transport, in *Communications in Hydraulics*, pp. 83–87, Delft Univ. of Technol., Delft, Netherlands, 1983.

Galappatti, G., and C. B. Vreugdenhil, A depth-integrated model for suspended sediment transport, *J. Hydraul. Res*., *23*, 359–376, 1985.

Galperin, B., and G. L. Mellor, A time-dependent, three-dimensional model of the Delaware Bay and River, part 1. Description of the model and tidal analysis, *Estuarine Coastal Shelf Sci*., *31*, 231–253, 1990.

Garcia, M. H., and G. Parker, Entrainment of bed sediment into suspension, *J. Hydraul. Eng*., *117*, 414–435, 1991.

Gottlieb, E. S., J. H. Saylor, and G. S. Miller, Currents and temperatures observed in Lake Michigan from June 1982 to July 1983, *NOAA Tech. Memo. ERL GLERL-71*, 45 pp., Great Lakes Environ. Res. Lab., Ann Arbor, Mich., 1989.

Grant, W. D., and O. S. Madsen, Combined wave and current interaction with a rough bottom, *J. Geophys. Res*., *84*, 1797–1808, 1979.

Hawley, N., Preliminary observations of sediment erosion from a bottom resting flume, *J. Great Lakes Res*., *17*, 361–367, 1991.

Hawley, N., and C. H. Lee, Sediment resuspension and transport in Lake Michigan during the unstratified period, *Sedimentology*, *46*, 791–806, 1999.

Hawley, N., and B. M. Lesht, Does resuspension maintain the benthic nepheloid layer in southeastern Lake Michigan? *J. Sediment. Res*., *Sect. A*, *65*, 69–76, 1995.

Hawley, N., and J. E. Zyrem, Transparency calibration for Lake St. Clair and Lake Michigan, *J. Great Lakes Res*., *16*, 113–120, 1990.

Hubertz, J. M., D. B. Driver, and R. D. Reinhard, Hindcast wave information for the Great Lakes: Lake Michigan, *WIS Rep. 24*, U.S. Army Corps of Eng., Washington, D. C., 1991.

Jibson, R. W., J. K. Odum, and J. Staude, Rates and processes of bluff recession along the Lake Michigan shoreline in Illinois, *J. Great Lakes Res*., *20*, 135–152, 1994.

Jonsson, I. G., Wave boundary layer and friction factors, paper presented at 10th Conference on Coastal Engineering, Am. Soc. of Civ. Eng., Tokyo, 1966.

Lee, C. H., and N. Hawley, The response of suspended particulate material to upwelling and downwelling events in southern Lake Michigan, *J. Sediment. Res*., *68*, 819–831, 1998.

Lee, D. H., K. W. Bedford, and C. J. Yen, Storm and entrainment effects on tributary sediment loads, *J. Hydraul. Eng*., *120*, 81–103, 1994.

Lesht, B. M., and N. Hawley, Near-bottom currents and suspended sediment concentration in southeastern Lake Michigan, *J. Great Lakes Res*., *13*, 375–386, 1987.

Lick, W., J. Lick, and C. K. Ziegler, The resuspension and transport of fine-grained sediments in Lake Erie, *J. Great Lakes Res*., *20*, 599–612, 1994.

Liu, P. C., D. J. Schwab, and J. R. Bennett, Comparison of a two-dimensional wave prediction model with synoptic measurements in Lake Michigan, *J. Phys. Oceanogr*., *14*(9), 1514–1518, 1984.

Lou, J., Modelling of hydrodynamics and suspended sediment transport in coastal areas, Ph.D. thesis, 243 pp., James Cook U., Townsville, Queensland, Australia, 1995.

Lou, J., and P. Ridd, Wave-current bottom shear stresses and sediment resuspension in Cleveland Bay, Australia, *Coastal Eng*., *29*, 169–186, 1996.

Lou, J., and P. Ridd, Modeling of suspended sediment transport in coastal areas under waves and current, *Estuarine Coastal Shelf Sci*., *45*, 1–16, 1997.

Lou, J., T. Wolf, and W. Rosenthal, Modeling sediment resuspension in coastal areas, in *Computerized Modeling of Sedimentary Systems*, edited by J. Harff, et al., pp. 23–35, Springer-Verlag, New York, 1999.

Mellor, G. L., Numerical simulation and analysis of the mean coastal circulation off California, *Con. Shelf Res*., *6*, 689–713, 1986.

Mellor, G. L., and T. Yamada, Development of a turbulence closure model for geophysical fluid problems, *Rev. Geophys*., *20*, 851–875, 1982.

Oey, L.-Y., G. L. Mellor, and R. I. Hires, A three-dimensional simulation of the Hudson-Raritan Estuary, part II, Comparison with observation, *J. Phys. Oceanogr*., *15*, 1693–1709, 1985.

Rakha, K. A., R. Deigaard, and I. Broker, A phase-resolving cross shore sediment transport model for beach profile evolution, *Coastal Eng*., *31*, 231–261, 1997.

Rao, D. B., and T. S. Murty, Calculation of the steady-state wind-

driven circulation in Lake Ontario, *Arch. Meteorol. Geophys. Bioklimatol*., *Ser. A*, *19*, 195–210, 1970.
Robbins, J. A., and B. J. Eadie, Seasonal cycling of trace elements, Cs-137, Be-7 and Pu-239+240 in Lake Michigan, *J. Geophys. Res*., *96*, 17,081–17,104, 1991.
Saylor, J. H., J. C. K. Huang, and R. O. Reid, Vortex modes in Lake Michigan, *J. Phys. Oceanogr*., *10*, 1814–1823, 1980.
Schwab, D. J., Numerical simulation of low-frequency current fluctuations in Lake Michigan, *J. Phys. Oceanogr*., *13*, 2213–2224, 1983.
Schwab, D. J., and K. W. Bedford, Initial implementation of the Great Lakes forecasting system: A real-time system for predicting lake circulation and thermal structure, *Water Pollut. Res. J. Can*., *29*, 203–220, 1994.
Schwab, D. J., and D. Beletsky, Lake Michigan mass balance study: Hydrodynamic modeling project, *NOAA Tech. Memo. ERL GLERL-108*, 53 pp., Great Lakes Environ. Res. Lab., Ann Arbor, Mich., 1998.
Schwab, D. J., and J. A. Morton, Estimation of overlake wind speed from overland wind speed: A comparison of three methods, *J. Great Lakes Res*., *10*, 68–72, 1984.
Schwab, D. J., J. R. Bennett, P. C. Liu, and M. A. Donelan, Application of a simple numerical wave prediction model to Lake Erie, *J. Geophys. Res*., *89*, 3586–3589, 1984.
Schwab, D. J., W. P. O'Connor, and G. L. Mellor, On the net cyclonic circulation in large stratified lakes, *J. Phys. Oceanogr*., *25*, 1516–1520, 1995.
Schwab, D. J., D. Beletsky, and J. Lou, The 1998 coastal turbidity plume in Lake Michigan, *Estuarine Coastal Shelf Sci*., in press, 1999.
Signell, R. P., R. C. Beardsley, H. C. Graber, and A. Capotondi, Effect of wave-current interaction on wind-driven circulation in narrow, shallow embayments, *J. Geophys. Res*., *95*, 9671–9678, 1990.
Simons, T. J., The mean circulation of unstratified bodies driven by nonlinear topographic wave interactions, *J. Phys. Oceanogr*., *16*, 1138–1142, 1986.
Strong, A. E., and B. J. Eadie, Satellite observations of calcium carbonate precipitations in the Great Lakes, *Limnol. Oceanogr*., *23*, 877–887, 1978.
Taylor, C. L., W. Lick, J. Boles, and E. Marschall, Erosion properties of Great Lakes sediments, Master thesis, 101 pp., Univ. of Calif., Santa Barbara, 1996.
Thorn, M. F. C., and J. G. Parsons, Erosion of cohesive sediments in estuaries, in *Proceedings of the third International Symposium on Dredging Technology*, *Bordeaux, France*, *5–7 March 1980*, edited by H. S. Stephens and C. A. Stapleton, pp. 123–132, BHRA Fluid Eng., Cranfield, Eng., 1980.
Tsai, C.-H., and W. Lick, A portable device for measuring sediment resuspension, *J. Great Lakes Res*., *12*, 314–321, 1986.
Van Rijn, L. C., Two-dimensional vertical mathematical model for suspended sediment transport by currents and waves, *Rep. S488-IV*, Delft Hydraul. Lab., Delft, Netherlands, 1985.
Van Rijn, L. C., Mathematical modeling of suspended sediment in nonuniform flows, *J. Hydraul. Eng*., *112*, 433–455, 1986.
Van Rijn, L. C., Sediment transport by currents and waves, *Rep. H461*, Delft Hydraul. Lab., Delft, Netherlands, 1989.
Wang, Z. B., and J. S. Ribberink, The validity of a depth-integrated model for suspended sediment transport, *J. Hydraul. Res*., *24*, 53–67, 1986.
Weatherly, G. L., and P. J. Martin, On the structure and dynamics of the ocean bottom boundary layer, *J. Phys. Oceanogr*., *8*, 557–570, 1978.
Wunsh, C., On the mean drift in large lakes, *Limnol. Oceanogr*., *18*, 793–795, 1973.
Ziegler, C. K., and W. Lick, A numerical model of the resuspension, deposition and transport of fine-grained sediments in shallow water, *UCSB Rep. ME-86-3*, Univ. of Calif., Santa Barbara, 1986.
Ziegler, C. K., and W. Lick, The transport of fine-grained sediments in shallow waters, *Environ. Geol. Water Sci*., *11*, 123–132, 1988.
Ziegler, C. K., and B. Nisbet, Fine-grained sediment transport in Pawtuxet River, Rhode Island, *J. Hydraul. Eng*., *120*, 561–576, 1994.

D. Beletsky, N. Hawley, J. Lou, and D. J. Schwab, Great Lakes Environmental Research Laboratory, 2205 Commonwealth Blvd., Ann Arbor, MI 48105-2945. (beletsky@glerl.noaa.gov; lou@glerl.noaa.gov; schwab@glerl.noaa.gov)

(Received December 9, 1998; revised August 12, 1999;
accepted November 10, 1999.)